

Central Lancashire Online Knowledge (CLoK)

Title	Adsorption and Thermal Stability of Ionic Liquid Multilayers on ZnO surfaces
Type	Article
URL	https://clock.uclan.ac.uk/55159/
DOI	https://doi.org/10.3390/surfaces8020029
Date	2025
Citation	Henderson, Zoë, Cole, Jordan, Thomas, Andrew G., Jones, Robert G., Wagstaffe, Michael, Avila, José, Asensio, María, Li, Zheshen and Syres, Karen orcid iconORCID: 0000-0001-7439-475X (2025) Adsorption and Thermal Stability of Ionic Liquid Multilayers on ZnO surfaces. <i>Surfaces</i> , 8 (2). p. 29.
Creators	Henderson, Zoë, Cole, Jordan, Thomas, Andrew G., Jones, Robert G., Wagstaffe, Michael, Avila, José, Asensio, María, Li, Zheshen and Syres, Karen

It is advisable to refer to the publisher's version if you intend to cite from the work.
<https://doi.org/10.3390/surfaces8020029>

For information about Research at UCLan please go to <http://www.uclan.ac.uk/research/>

All outputs in CLoK are protected by Intellectual Property Rights law, including Copyright law. Copyright, IPR and Moral Rights for the works on this site are retained by the individual authors and/or other copyright owners. Terms and conditions for use of this material are defined in the <http://clock.uclan.ac.uk/policies/>

Article

Adsorption and Thermal Stability of Ionic Liquid Multilayers on ZnO Surfaces

Zoë Henderson ^{1,*},[†], Jordan Cole ^{1,‡}, Andrew G. Thomas ^{2,3}, Robert G. Jones ⁴, Michael Wagstaffe ^{5,§}, José Avila ⁶, María C. Asensio ^{6,7}, Zheshen Li ⁸ and Karen L. Syres ^{1,4,*}

- ¹ Jeremiah Horrocks Institute for Mathematics, Physics and Astronomy, University of Central Lancashire, Preston PR1 2HE, UK
- ² Department of Materials and Photon Science Institute, University of Manchester, Manchester M13 9PL, UK; andrew.g.thomas@manchester.ac.uk
- ³ The Henry Royce Institute, University of Manchester, Manchester M13 9PL, UK
- ⁴ School of Chemistry, University of Nottingham, Nottingham NG7 2RD, UK; profrobjones@me.com
- ⁵ Department of Physics and Astronomy, University of Manchester, Manchester M13 9PL, UK; michael.wagstaffe@iaf.fraunhofer.de
- ⁶ Synchrotron SOLEIL, L'Orme des Merisiers, 91190 Saint-Aubin, France; jose.avila@synchrotron-soleil.fr (J.A.); mc.asensio@csic.es (M.C.A.)
- ⁷ GREENER Group, Institute of Materials Science of Madrid (ICMM), Spanish National Research Council (CSIC) & MATINÉE: CSIC Associated Unit Between the Institute of Materials Science at the University of Valencia (ICMUV) and ICMM, 28049 Madrid, Spain
- ⁸ Department of Physics and Astronomy, University of Aarhus, Ny Munkegade, DK-8000 Aarhus C, Denmark; zshli@phys.au.dk
- * Correspondence: zoe.henderson@nsg.com (Z.H.); ksyres@uclan.ac.uk (K.L.S.)
- † Current address: NSG Group, European Technical Centre, Hall Lane, Lathom, Ormskirk, Lancashire L40 5UF, UK.
- ‡ Current address: Nanoco Technologies Ltd., Science Centre, The Heath Business & Technical Park, Runcorn, WA7 4QX, UK.
- § Current address: Fraunhofer Institute for Applied Solid State Physics IAF, Tullastraße 72, 79108 Freiburg, Germany.

Abstract: Ionic liquids (ILs) have been explored as a way of improving the performance of ZnO-based optoelectronic devices; however, there are few fundamental studies of the IL/ZnO interface. Here, the adsorption of the IL 1-octyl-3-methylimidazolium tetrafluoroborate [C₈C₁Im][BF₄] on ZnO (0001) and ZnO (10 $\bar{1}$ 0) has been studied using synchrotron-based soft X-ray photoelectron spectroscopy. The results indicate that [C₈C₁Im][BF₄] is deposited intact on the ZnO (0001) surface; however, there is some dissociation of [BF₄][−] anions, resulting in boron atoms attaching to the oxygen atoms in the ZnO surface and forming B₂O₃. In contrast, the deposition of [C₈C₁Im][BF₄] on the ZnO (10 $\bar{1}$ 0) surface at −150 °C results in the appearance of more chemical environments in the spectra. We propose that the high temperature of the IL evaporator causes some conversion of [C₈C₁Im][BF₄] to a carbene–borane adduct, resulting in the deposition of both the IL and adduct onto the ZnO surface. The adsorption and desorption of the analogous IL 1-butyl-3-methylimidazolium tetrafluoroborate [C₄C₁Im][BF₄] was investigated on ZnO (0001) using synchrotron-based soft X-ray photoelectron spectroscopy. The results indicate that [C₄C₁Im][BF₄] is deposited largely intact at −150 °C and forms islands when heated to room temperature. When heated to over 80 °C, it begins to react with the ZnO surface and decomposes. This is a much lower temperature than the long-term thermal stability of the pure IL, quoted in the literature as ~400 °C, and of IL on powdered ZnO, quoted in the literature as ~300 °C. This indicates that the ZnO surface may catalyse the thermal decomposition of [C₄C₁Im][BF₄] at lower temperatures. This is likely to have a negative impact on the potential use of ILs in ZnO-based photovoltaic applications, where operating temperatures can routinely reach 80 °C.



Academic Editor: Stefano Fabris

Received: 7 March 2025

Revised: 28 March 2025

Accepted: 14 April 2025

Published: 25 April 2025

Citation: Henderson, Z.; Cole, J.; Thomas, A.G.; Jones, R.G.; Wagstaffe, M.; Avila, J.; Asensio, M.C.; Li, Z.; Syres, K.L. Adsorption and Thermal Stability of Ionic Liquid Multilayers on ZnO Surfaces. *Surfaces* **2025**, *8*, 29. <https://doi.org/10.3390/surfaces8020029>

Copyright: © 2025 by the authors. Licensee MDPI, Basel, Switzerland. This article is an open access article distributed under the terms and conditions of the Creative Commons Attribution (CC BY) license (<https://creativecommons.org/licenses/by/4.0/>).

Keywords: ionic liquid; ZnO (0001); ZnO (10 $\bar{1}$ 0); XPS; multilayers; thin film; thermal decomposition

1. Introduction

ZnO is an n-type semiconductor and is a desirable material for optoelectronic applications due to its direct wide band gap of ~ 3.3 eV at 300 K and large exciton binding energy (~ 60 meV) [1]. It is stable, non-toxic and relatively cheap to manufacture in bulk quantities [1,2]. ZnO is also used in catalysis and can be utilised in a variety of applications, including methanol synthesis [3], water treatment [4] and H₂O/CO₂ splitting [5].

In optoelectronic devices, particularly organic-based devices, the main challenge lies in lowering the charge transfer barrier between the active layer and the metal oxide layer. This is achieved by engineering the energy difference between the conduction band of the metal oxide and the lowest unoccupied molecular orbital (LUMO) of the active layer [6]. This can be performed using an organic electrolyte, located between the metal oxide and the active layer, to enhance charge transfer. Charge transfer across an interface is closely linked to the arrangement of atoms or molecules at the interface in question. Lee et al. [7] showed that modifying n-type ZnO with a monolayer of ionic liquid (IL) (1-benzyl-3-methylimidazolium chloride) can enhance the performance of hybrid organic–inorganic polymeric light-emitting diodes and solar cells. ILs are salts, composed solely of anions and cations, held together by their Coulomb potential. Unlike inorganic salts, they tend to be liquid at room temperature due to their large, asymmetric ions. There are millions of possible combinations of ions, and these can be tuned to achieve desired chemical properties. For example, some ILs might react with ZnO, whilst others may not. In the study by Lee et al. [7], the ZnO layer in the devices was 80 nm thick and prepared by spray pyrolysis from zinc acetate dihydrate/methanol precursor solutions. For the IL-modified ZnO layer, the IL was dissolved in water and spin-coated onto the ZnO layer and annealed to remove residual water. The IL ions were found to self-assemble, with the Cl anions located at the ZnO surface and the 1-benzyl-3-methylimidazolium cations at the active layer. This dipole arrangement shifts the conduction band minimum of ZnO closer to that of the active layer, subsequently causing a decrease in the ZnO work function and the charge transfer barrier [6,7]. The self-assembly, low vapour pressure and ionic nature of ILs, therefore, provide an advantage in the potential application to photovoltaic systems relative to other organic electrolytes. The organic electrolytes, traditionally used in dye-sensitised solar cells (DSSCs), tend to have a high vapour pressure that results in evaporation over time [8], which can be accelerated by solar heating. These devices, therefore, typically require an upper limit for the working temperature of solar cells to be around 85 °C [9,10]. The decomposition and evaporation of the electrolyte result in decreased conversion efficiencies or even short-circuiting. In contrast, ILs do not evaporate under these conditions, so they may offer a solution to the loss of electrolytes in solar devices. It is important to understand the interactions at the interface between the electrolyte and the semiconductor at high temperatures, which is the focus of this study.

IL/metal oxide interfaces are also important in IL catalysis applications. Supported ionic liquid phase (SILP) catalysis consists of a thin layer of IL containing a catalyst spread over a high-surface-area support. A solid catalyst with an ionic liquid layer (SCILL) uses a solid heterogeneous catalyst coated with a thin layer of IL. In these applications, the IL is used to tune the selectivity of the catalyst and to increase the concentration of reactants at the surface through the absorption of the reactants into the IL. Interactions between the IL and the catalyst itself, however, could alter the adsorption and/or reaction prop-

erties of the catalyst. Sobota et al. [11,12] conducted a combined IR absorption and X-ray photoelectron spectroscopy (XPS) study into the effects of 1-butyl-3-methylimidazolium bis(trifluoromethylsulphonyl)imide, $[C_4C_1Im][Tf_2N]$, on CO adsorption on Pd nanoparticles immobilised on an Al_2O_3 support. The addition of IL to the system reduced CO adsorption at bridge sites on the catalyst but stabilised adsorption on the hollow sites of facet features on the catalyst. More importantly, they found that the IL decomposed when the system was heated, and the decomposition products blocked the majority of the CO adsorption sites on the Pd catalysts. XPS revealed that the decomposition species (which were cation-derived) were preferentially located on the catalyst nanoparticles and not on the Al_2O_3 support, resulting in poisoning of the catalyst.

The three crystal structures of ZnO are wurtzite, zinc blende and rock salt. At ambient conditions, the thermodynamically stable phase of ZnO is wurtzite. The wurtzite structure has a hexagonal unit cell described by four axes, three of equal length in the basal plane (orientated at 120° to each other) and one normal to this plane [1]. This forms a hexagonal prism shape described by four-index notation ($a = 3.25 \text{ \AA}$, $c = 5.206 \text{ \AA}$). The non-polar ZnO $(10\bar{1}0)$ surface is perpendicular to the basal plane (parallel to the length of the prism) and is terminated by equal numbers of Zn^{2+} and O^{2-} atoms. In UHV, a clean ZnO $(10\bar{1}0)$ surface shows flat rectangular terraces separated by single-layer height steps ($\sim 3 \text{ \AA}$) [13]. The polar ZnO $(000\bar{1})$ surface is parallel to the basal plane and is dominated by O^{2-} atoms (referred to as O terminated). In UHV, a clean ZnO (0001) surface shows flat hexagonal terraces separated by double-layer height steps ($\sim 5.3 \text{ \AA}$). The polar ZnO (0001) surface is also parallel to the basal plane but is dominated by Zn^{2+} atoms (referred to as Zn terminated). In UHV, a clean ZnO (0001) -Zn surface shows triangular terraces covered by a high density of triangular islands and pits with single-layer height steps ($\sim 2.7 \text{ \AA}$) [13]. A dipole moment is created perpendicular to the (0001) and $(000\bar{1})$ polar surfaces. In this study, we use the ZnO (0001) -Zn polar surface. To stabilise the (0001) surface, it has been found that 25% of Zn atoms must be removed from the surface, which exposes O atoms at the step edges of the triangular islands and pits [14]. Therefore, the step edges on the (0001) surface are O-terminated [13]. The undercoordinated Zn cations at the surface act as active sites for adsorption, so the (0001) surface is usually more reactive than the $(000\bar{1})$ surface. The (0001) plane has the lowest surface free energy and is the most favourable plane in polycrystalline ZnO powder [15,16].

There are very few studies in the literature on the interaction between ionic liquids and single-crystal ZnO surfaces [17]. Kanai et al. performed electrochemical measurements across the ZnO $(000\bar{1})$ -O single-crystal/IL interface and confirmed good stability of the interface using reflection high energy electron diffraction (RHEED) measurements before and after electrochemical measurements [18]. Current studies in the literature focus on the interaction of ILs with ZnO nanostructures and their performance in devices [17].

Here, we present the first investigation into the adsorption of the IL 1-octyl-3-methylimidazolium tetrafluoroborate, $[C_8C_1Im][BF_4]$, on single-crystal non-polar ZnO $(10\bar{1}0)$ and polar ZnO (0001) -Zn in vacuum using XPS at the ANTARES beamline at the SOLEIL synchrotron [19]. The thermal stability of the analogous IL 1-butyl-3-methylimidazolium tetrafluoroborate, $[C_4C_1Im][BF_4]$, on polar ZnO (0001) was studied using XPS at the AU-MatLine beamline at the ASTRID2 synchrotron [20] over a temperature range of $-150 \text{ }^\circ\text{C}$ to $200 \text{ }^\circ\text{C}$. The only difference between the two ILs is the length of the alkyl chain on the imidazolium cation. The chemistry of the two ILs will be the same, but their steric effects may be different.

2. Materials and Methods

2.1. $[C_8C_1Im][BF_4]$ on Polar ZnO (0001)–Zn and Non-Polar ZnO (10 $\bar{1}0$)

This experiment was carried out at the ANTARES beamline at the SOLEIL synchrotron in Saint-Aubin, France. The ZnO (0001) and (10 $\bar{1}0$) single-crystal surfaces (5 mm × 10 mm, PI-KEM, Tamworth, UK) were mounted onto Ta sample plates and fixed into place with Ta wire. They were cleaned via several Ar⁺ sputter–anneal cycles (sputtering at 1 keV for 15 min and annealing at 700 °C for 20 min) with a final anneal at 700 °C in 10^{−6} mbar O₂ for five minutes to replace the preferentially sputtered O atoms and restore the stoichiometry of the surface. The cleanliness of the surfaces was determined by XPS (see Supporting Information (SI), Figure S1). The low-energy electron diffraction (LEED) pattern was acquired for the ZnO (0001) surface to confirm long-range order and structure for the (0001) termination. The LEED pattern exhibited sharp diffraction beams on a low intensity background, indicating a well-ordered (0001) surface with few defects (see SI, Figure S2).

The IL, 1-octyl-3-methylimidazolium tetrafluoroborate ($[C_8C_1Im][BF_4]$, Sigma Aldrich, Gillingham, UK, >97%, shown in Figure 1) was degassed in vacuo in a modified Knudsen cell at 120 °C for approximately 3 h to remove water and impurities (see SI for details of the modified Knudsen cell, Figure S3). The IL was heated to ~350 °C for deposition; however, the thermocouple was in contact with the metal shell of the evaporator, not the IL itself, so we expect the real temperature of the IL to be lower than this. Using a combination of the TPP-2M calculation for the inelastic mean free path for organic materials [21] and the Beer–Lambert relation for photoelectron attenuation in thin films [22], the thicknesses of the IL depositions were calculated by monitoring the attenuation of the Zn 3p_{3/2} substrate peaks following deposition (refer to “IL deposition thickness and probing depth calculations” in SI for details and Table S1 for a summary of the calculated thicknesses). The IL layer thickness on ZnO (0001) was found to be approximately (11.3 ± 0.4) Å, corresponding to an estimated 1.6 IL layers, assuming the “thickness” of one $[C_8C_1Im][BF_4]$ pair to be ~7 Å [23]. The IL layer thickness on ZnO (10 $\bar{1}0$) was found to be approximately (6.3 ± 0.4) Å. This corresponds to approximately 0.9 IL layers, suggesting a sub-monolayer coverage. Alternatively, it could be that ~1 ML of IL has been formed on each ZnO surface, but the IL adsorption geometry is different because of the difference between the polar and non-polar surfaces. On the polar ZnO (0001) surface, the BF₄[−] anions could form a layer on top of the Zn²⁺ layer, and the $[C_8C_1Im]^+$ cations form a layer on top of that (i.e., Zn²⁺/BF₄[−]/ $[C_8C_1Im]^+$), whereas on the non-polar ZnO (10 $\bar{1}0$) surface, there may be a checkerboard of anions and cations that are coplanar, with the C₈ aliphatic chains sticking upwards, making the overall IL layer thinner. However, it is not possible to conclusively determine the geometry from our XPS results.

Initial beam damage studies showed small changes in spectra with time under the X-ray beam; therefore, to ameliorate beam damage, the samples were cooled to −150 °C and each XPS spectrum was taken at a new position on the surface. The IL was deposited on the polar ZnO (0001) substrate at room temperature and then cooled to −150 °C, whereas the non-polar ZnO (10 $\bar{1}0$) substrate was cooled to −150 °C prior to IL deposition. Beam damage studies at −150 °C showed no change in spectra under the X-ray beam over a typical length scan. Cooling the sample increases the risk of residual water condensing on the surface of the ZnO/IL, and this is discussed in the results. XPS measurements were taken at normal emission (surface facing the analyser) with the incident X-ray beam at 45° to the surface normal. Measurements have been calibrated on the binding energy (BE) scale to the O 1s region for ZnO at 530.0 eV [24]. All core level XPS BEs are quoted to ±0.1 eV.

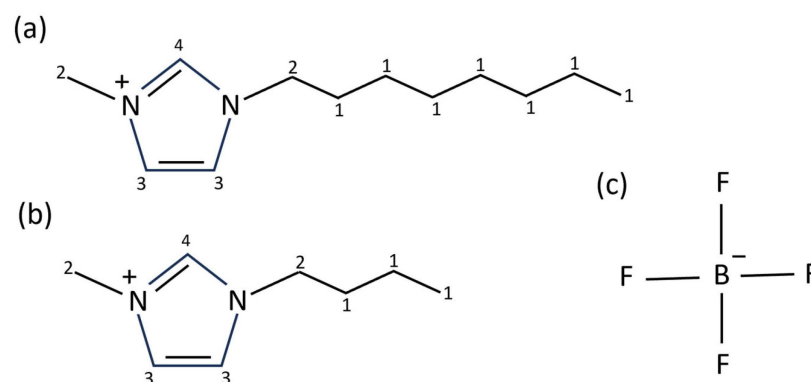


Figure 1. The structure of the composite ions of the ILs used in this study. (a) is the $[\text{C}_8\text{C}_1\text{Im}]^+$ cation, (b) is the $[\text{C}_4\text{C}_1\text{Im}]^+$ cation, and (c) is the $[\text{BF}_4]^-$ anion. The carbon atoms in each cation have been numbered 1–4 to highlight the different carbon environments (these are referred to as C1–C4 throughout the paper).

2.2. $[\text{C}_4\text{C}_1\text{Im}][\text{BF}_4]$ on Polar ZnO (0001)

These experiments took place at the AU-MatLine beamline at ASTRID2 synchrotron in Aarhus, Denmark. The polar ZnO (0001) single-crystal substrate (5 mm × 5 mm, PI-KEM) was mounted on a Ta sample plate and held in place by Ta strips. The substrate was prepared in the same way as described above. Similarly, a LEED pattern was acquired for the ZnO (0001) crystal (see SI, Figure S2), which confirmed that the ZnO (0001) had the correct surface termination and good long-range order. 1-butyl-3-methylimidazolium tetrafluoroborate ($[\text{C}_4\text{C}_1\text{Im}][\text{BF}_4]$, Sigma Aldrich, Gillingham, UK, >97%, shown in Figure 1) was degassed in vacuo in a modified Knudsen cell at $\sim 120^\circ\text{C}$ for three hours to remove water and impurities. The IL was heated to 180°C for deposition, measured from a thermocouple placed inside the glass vial containing the IL (see SI for details of the modified Knudsen cell, Figure S3). The ZnO (0001) substrate was cooled to -150°C prior to IL deposition. The $[\text{C}_4\text{C}_1\text{Im}][\text{BF}_4]$ deposition on ZnO (0001) was found to be approximately $(15.2 \pm 0.3) \text{ \AA}$, corresponding to an estimated 3.8 IL layers, assuming the “thickness” of one $[\text{C}_4\text{C}_1\text{Im}][\text{BF}_4]$ pair to be $\sim 4 \text{ \AA}$ [25].

XPS spectra were recorded as the sample was heated from -150°C , through the glass transition temperature of $[\text{C}_4\text{C}_1\text{Im}][\text{BF}_4]$ (-97°C [26]), up to 200°C (two preliminary temperature runs were carried out to observe trends in the data before preparing a fresh IL film and recording the data presented here). At each temperature, spectra were taken at normal emission (NE) and 45° emission (referred to as grazing emission, GE). At NE, the incident X-ray beam was at 45° to the surface normal, with the surface facing the analyser. At 45° emission (GE), the surface was facing the incident X-ray beam and was at 45° to the analyser (i.e., the incident X-ray beam and analyser are 45° apart). Using the equation for probing depth (with a mean free path of 4.3 \AA for $[\text{C}_4\text{C}_1\text{Im}][\text{BF}_4]$), measurements taken at NE and GE were calculated to have sampling depths of 1.5 nm and 1.0 nm, respectively [21,27], i.e., the GE spectra have higher surface sensitivity (see SI for calculation). Initial beam damage studies showed no change in spectra under the X-ray beam over a typical length scan. The binding energies of core level XPS peaks have been calibrated to the Zn $3p_{3/2}$ peak at 88.6 eV [28] and are quoted to $\pm 0.1 \text{ eV}$ (Zn $3p_{3/2}$ was used for calibration in these experiments because the O 1s ZnO feature at 530 eV was difficult to resolve in low-temperature spectra).

3. Results

3.1. $[\text{C}_8\text{C}_1\text{Im}][\text{BF}_4]$ Adsorbed on ZnO (0001) at RT and ZnO (10 $\bar{1}$ 0) at -150°C

$[\text{C}_8\text{C}_1\text{Im}][\text{BF}_4]$ was deposited on the ZnO (0001) substrate at room temperature and then cooled to -150°C , whereas the ZnO (10 $\bar{1}$ 0) substrate was cooled to -150°C prior to

[C₈C₁Im][BF₄] deposition. The core level XPS of [C₈C₁Im][BF₄] on ZnO (0001) and ZnO (10 $\bar{1}$ 0) are shown in Figure 2, and a summary of fitted peaks and assignments is shown in Table 1. On the ZnO (0001) surface, the IL appears to be deposited intact. On the ZnO (10 $\bar{1}$ 0) surface, the XPS results suggest a different species is deposited on the surface. We propose this species is a carbene–borane adduct formed in the evaporator, as discussed further below.

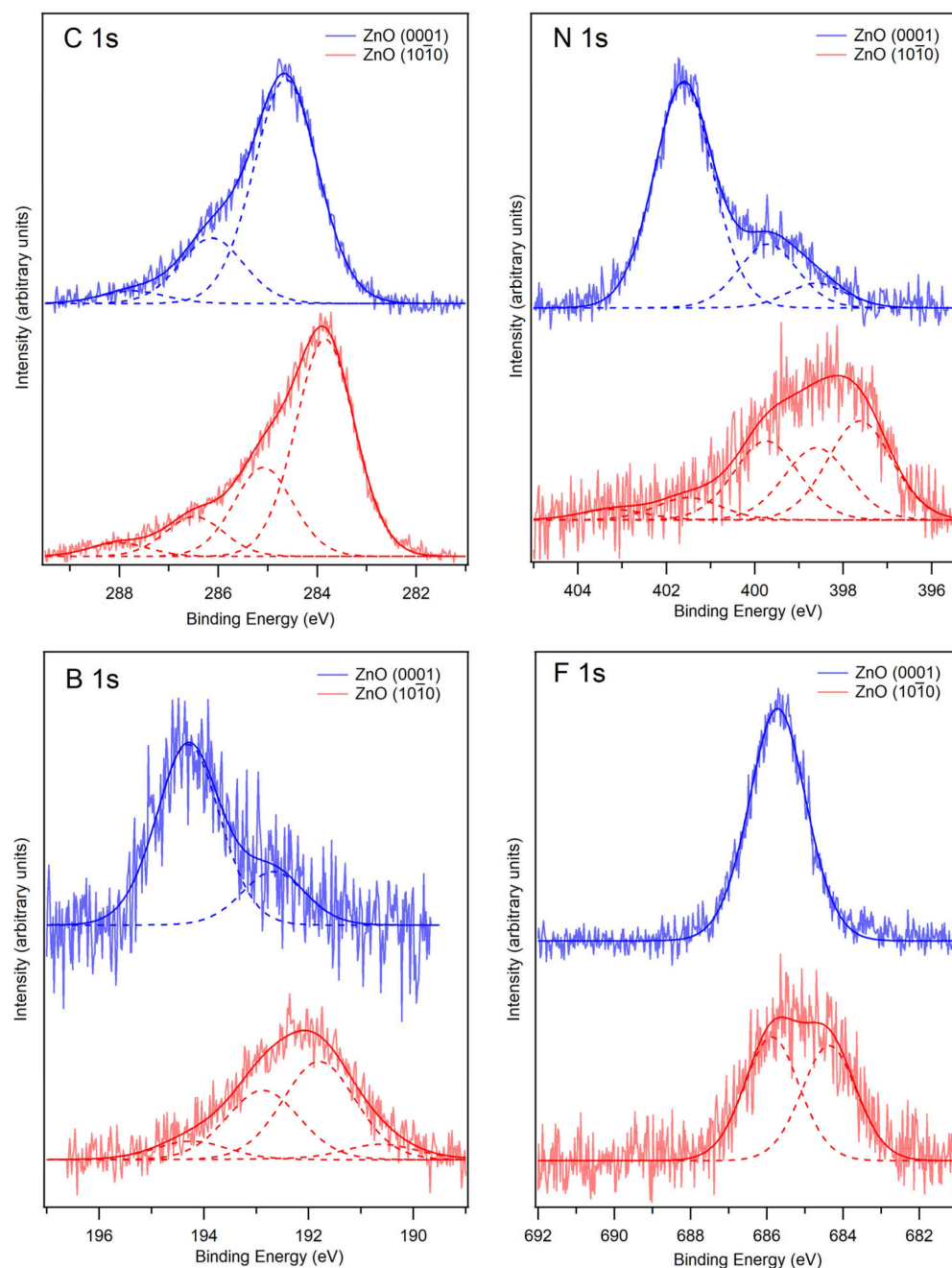


Figure 2. Core level XPS of [C₈C₁Im][BF₄] on ZnO (0001) (blue curves) and ZnO (10 $\bar{1}$ 0) (red curves). The IL was deposited on the ZnO (0001) substrate at room temperature and then cooled to -150 °C, whereas the ZnO (10 $\bar{1}$ 0) substrate was cooled to -150 °C prior to IL deposition. Fitted components are shown by dashed lines, and the resultant envelope is shown by a darker solid line. The C 1s region is normalised to the largest peak intensity, and the N 1s, F 1s and B 1s regions are normalised to the total region area. The photon energies used for each region were as follows: 700 eV for the C 1s and N 1s regions, 800 eV for the F 1s region and 300 eV for the B 1s region.

Table 1. Summary of fitted peaks for $[C_8C_1Im][BF_4]$ on ZnO (0001) and on ZnO ($10\bar{1}0$).

Region	BE (eV) (± 0.1 eV)		Assignment
	ZnO (0001)	ZnO ($10\bar{1}0$)	
C 1s	284.6	283.8	C1 in Figure 1a *
	286.2	285.1	C2 + C3 in Figure 1a *
	287.8	286.5	C4 in Figure 1a
		288.0	CO/C attached to BF_3 in adduct
N 1s	398.6	397.6	Decomposition/beam damage
	399.7	398.6	Decomposition/beam damage
	401.6	399.8	N atoms in $[C_4C_1Im]^+$ cation
		401.5	Decomposition
		403.2	Decomposition
F 1s		684.4	F atom in BF_3 in adduct
	685.7	685.9	F atoms in $[BF_4]^-$ anion
B 1s		190.6	Decomposition product
		191.8	B atom in BF_3 in adduct
	192.7	192.9	B_2O_3
	194.3	194.3	B atom in $[BF_4]^-$ anion

* ZnO ($10\bar{1}0$) may have a mixture of the IL and carbene–borane adduct on the surface, so C1, C2 and C3 refer to carbon environments in both the IL (shown in Figure 1a) and the adduct (shown in Figure 3).

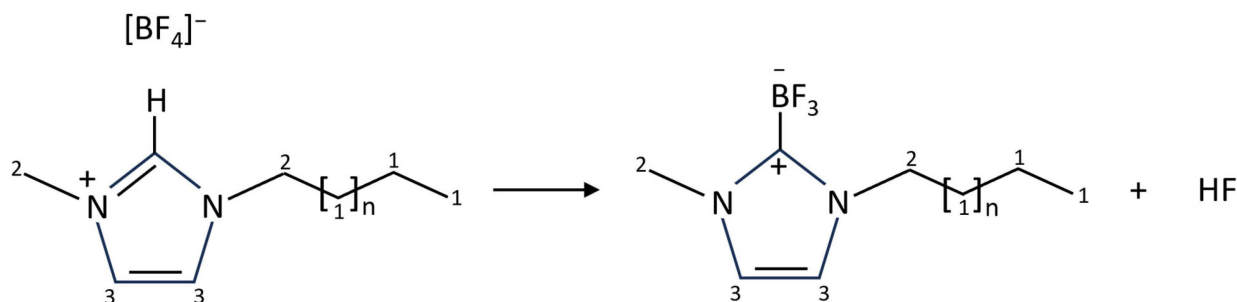


Figure 3. $[C_nC_1Im][BF_4]$ conversion to a carbene–borane adduct, in which the acidic H on the imidazole is replaced by BF_3 to produce 1-alkyl-3-methylimidazolium-2-trifluoroborate with elimination of HF. The carbon atoms have been numbered 1–3 to highlight the different carbon environments.

The C 1s spectra for $[C_8C_1Im][BF_4]$ on ZnO (0001) and ZnO ($10\bar{1}0$) are shown in Figure 2. For $[C_8C_1Im][BF_4]$ on ZnO (0001), three peaks are fitted at 284.6 eV, 286.2 eV and 287.8 eV. The most intense peak at 284.6 eV is attributed to carbon atoms in the alkyl chain of the imidazolium cation (carbon 1 in Figure 1a (C1)). The peak at 286.2 eV is attributed to carbon atoms that are attached to one N atom in the imidazolium cation (carbons 2 and 3 in Figure 1a (C2 + C3)). The peak at 287.8 eV is attributed to the carbon atom between the two N atoms in the imidazolium cation (carbon 4 in Figure 1a (C4)). The BE of these features are in good agreement with the values in the literature for this IL [29]. This indicates that the $[C_8C_1Im]^+$ ion adsorbs intact without dissociation on the (0001) surface. For $[C_8C_1Im][BF_4]$ on ZnO ($10\bar{1}0$), four peaks are required to produce a good fit to the data. These peaks are fitted at 283.8 eV, 285.1 eV, 286.5 eV and 288.0 eV. We assign the peaks at 283.8 eV, 285.1 eV and 286.5 eV to be the same carbon environments described for the ZnO (0001) surface but shifted to lower binding energies. The shift could be due to

relaxation effects during photoemission, which will be different for the two surfaces, or it could be that the IL has decomposed into another species (discussed below). The peak at 288.0 eV could be due to CO that adsorbed on the surface when it was cooled prior to deposition or from a decomposition species. For the (10 $\bar{1}0$) surface, we also observe an increase in intensity of the higher BE peaks relative to the alkyl chain peak (at 283.8 eV) when compared to the (0001) surface, which could be further indication of a decomposition species on the surface. If there is some intact IL on the surface, it is likely to adopt a different structure on the two surfaces. The IL was deposited at -150 °C on the (10 $\bar{1}0$) surface, where the IL is likely to form snow-like layers. The IL was deposited at room temperature on the (0001) surface, where the IL is liquid and can adopt a favourable structure before being frozen. It has been reported in the literature that this IL often orientates with its alkyl chains facing outwards towards the vacuum with the ring part of the cation residing beneath it [30–33] (see schematic model in Figure 4). The fact that the ZnO (0001) surface is polar may affect the ordering of the IL, possibly causing it to self-assemble as it aligns with the electric field of the substrate.

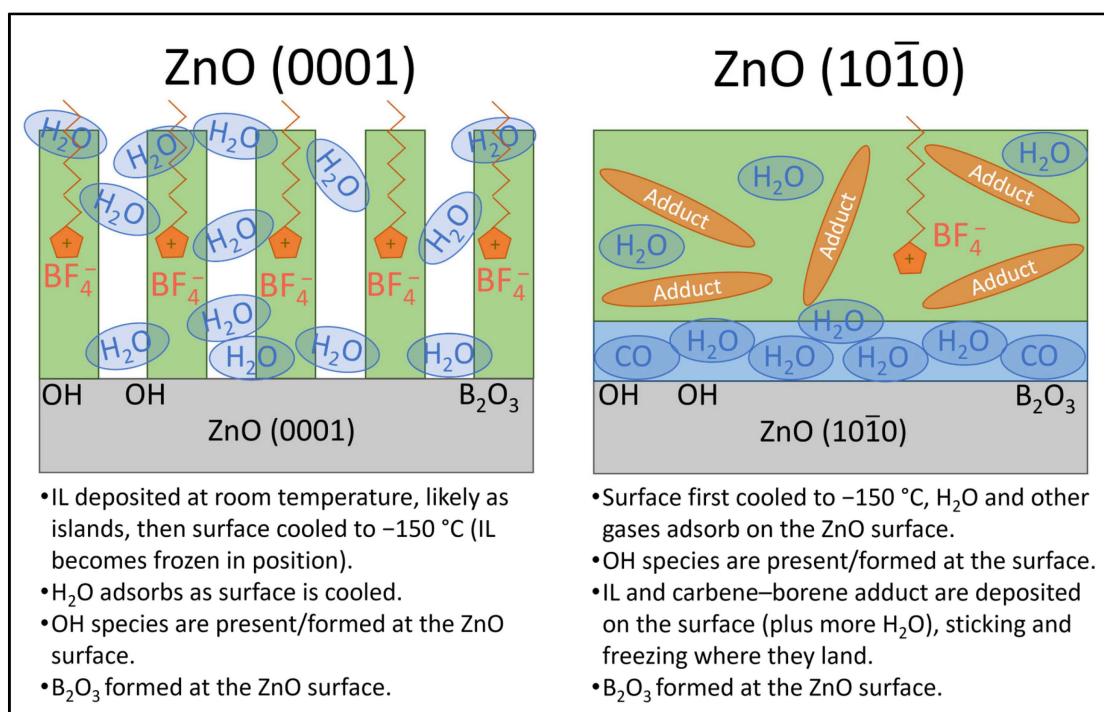


Figure 4. Schematic model showing the adsorption of [C₈C₁Im][BF₄] on ZnO (0001) and ZnO (10 $\bar{1}0$) surfaces.

A paper by A.W. Taylor et al. [34] showed that refluxing [C₄C₁Im][BF₄] or [C₈C₁Im][BF₄] at high temperatures under vacuum for extended periods of time resulted in the formation of a carbene–borane adduct (a borane-substituted imidazol-2-ylidene), in which the acidic H on the imidazole was replaced by BF₃ to produce 1-alkyl-3-methylimidazolium-2-trifluoroborate with elimination of HF (Figure 3). If this adduct was present on the ZnO (10 $\bar{1}0$) surface could explain the difference between the C 1s spectra. The overall carbene–borane adduct is neutral, and this could account for the observed shift to lower binding energies in the ZnO (10 $\bar{1}0$) spectra. The carbon atom attached to the BF₃ in the carbene–borane adduct would give rise to a high BE peak, which could explain the additional peak at 288.0 eV fitted to the ZnO (10 $\bar{1}0$) spectra. There could be a combination of the carbene–borane adduct and IL contributing to the C 1s spectrum. This adduct could have emanated directly from the evaporator, with the vapour emitted from the evaporator containing a mixture of the IL, adduct and HF. Since the ZnO (10 $\bar{1}0$) surface was at -150 °C during deposition, it is more likely the adduct would stick

to the surface, whereas the ZnO (0001) surface was at room temperature during deposition, where the adduct is less likely to stick (the adduct has a higher vapour pressure than the IL). In addition, the deposition time for the IL/ZnO (10 $\bar{1}0$) experiment was longer than that for the IL/ZnO (0001) experiment, so it may be more likely that the adduct formed in the evaporator and adsorbed on the ZnO (10 $\bar{1}0$) surface. Alternatively, it might be possible that the deposited IL reacted with the ZnO (10 $\bar{1}0$) surface forming the carbene–borane adduct, whereas it remained intact on the less reactive ZnO (0001) surface. However, the ZnO (10 $\bar{1}0$) surface was at -150 °C during IL deposition, so a reaction with the surface is energetically unlikely.

The N 1s spectra for [C₈C₁Im][BF₄] on ZnO (0001) and ZnO (10 $\bar{1}0$) are shown in Figure 2. For [C₈C₁Im][BF₄] on ZnO (0001), three peaks are fitted at 398.6 eV, 399.7 eV and 401.6 eV. The most intense peak at 401.6 eV is attributed to nitrogen atoms in the [C₈C₁Im]⁺ cation [29,35]. This value is in line with BE values in the literature for analogous ILs [29]. The [C₈C₁Im]⁺ cation consists of two nitrogen atoms, which are chemically equivalent due to resonance [29], and thus produce one signal in the N 1s region. The smaller peaks at 398.6 eV and 399.7 eV could arise from the decomposition of the IL on the surface. If the carbene–borane adduct is a decomposition product, the N atoms in the adduct are likely to produce a peak at lower binding energy than the N atoms in the IL since they have a relatively more negative charge. Alternatively, these lower BE peaks could arise from beam damage that occurred whilst taking measurements under the X-ray beam. For [C₈C₁Im][BF₄] on ZnO (10 $\bar{1}0$), five peaks are fitted to the N 1s spectrum at binding energies of 397.6, 398.6, 399.8, 401.5 and 403.2 eV. Due to the broad nature of the spectrum, it is difficult to fit peaks and make assignments with confidence. In the C 1s spectra, a shift to lower binding energy by approximately 1 eV was observed on the (10 $\bar{1}0$) surface relative to the (0001) surface, so one might expect a similar trend with the N 1s spectra. Therefore, the peak at 399.8 eV could be attributed to nitrogen atoms in the [C₈C₁Im]⁺ cation, which was assigned at 401.6 eV on the ZnO (0001) surface (although this is a larger shift than observed with the C 1s spectra). On the (0001) surface, the [C₈C₁Im]⁺ cation peak was the most intense, but on the (10 $\bar{1}0$) surface, its relative intensity is decreased, and the peak at 397.6 eV is the most intense. The number of N environments on the (10 $\bar{1}0$) surface suggests that the imidazolium ring could have broken up, with nitrogen atoms possibly attaching to the ZnO surface. If the carbene–borane adduct is present on the surface, there could be a combination of the IL, the carbene–borane adduct and other degradation products contributing to the N 1s spectrum.

The F 1s spectra for [C₈C₁Im][BF₄] on ZnO (0001) and ZnO (10 $\bar{1}0$) are shown in Figure 2. For [C₈C₁Im][BF₄] on ZnO (0001), one peak is fitted at a binding energy of 685.7 eV. The BE of this peak is consistent with F atoms in the [BF₄][−] anion [29], indicating that the IL is intact on the surface, which agrees with the C 1s data. The F 1s spectrum for [C₈C₁Im][BF₄] on ZnO (10 $\bar{1}0$) is broader than for the ZnO (0001) surface. It has been fitted with two peaks of similar intensity at 684.4 eV and 685.9 eV. The peak at 685.9 eV is assigned to the F atoms in the [BF₄][−] anion, as with the (0001) surface. The presence of an additional chemical species on the surface supports the C 1s and N 1s data, and we therefore assign the peak at 684.4 eV to F atoms in the BF₃ environment in the carbene–borane adduct. If the IL has decomposed, the F 1s spectrum could encompass a range of peaks at slightly different BEs, where F atoms could be bonded to C atoms or Zn atoms in the substrate. When the IL converts to the carbene–borane adduct, HF is also produced in the reaction. It is possible that HF impinging on the sample from the evaporator might stick to the surface at -150 °C. It has been shown that HF can adsorb on a Au (110) surface at -173 °C, giving rise to a F 1s peak at higher BE than the [BF₄][−] anion, which can easily desorb upon heating to -100 °C [36]. We see no evidence of a higher BE peak in our spectra, suggesting that the HF does not stick to the ZnO surface at -150 °C. If HF impinges on the walls of the UHV

chamber during dosing, it might displace H₂O and CO from the chamber walls, hence removing HF from the gas phase (resulting in no detectable HF signal on the surface) but increasing the flux of H₂O and CO hitting the surface.

The B 1s spectra for [C₈C₁Im][BF₄] on ZnO (0001) and ZnO (10 $\bar{1}$ 0) are shown in Figure 2. For [C₈C₁Im][BF₄] on ZnO (0001), two peaks have been fitted at 192.7 eV and 194.3 eV. The most intense peak at 194.3 eV is consistent with the B atom in the [BF₄][−] anion [29]. We propose that the smaller peak at 192.7 eV arises from dissociation of [BF₄][−] anions where B atoms attach to O^{2−} ions, which are exposed at step edges of the triangular islands and pits on the ZnO (0001) surface. This binding energy is consistent with B atoms in a B₂O₃ environment [37]. A reaction of the [BF₄][−] ion with OH groups on the surface might also have occurred, forming HF. However, this would desorb from the surface at room temperature, so it would not be visible in spectra. For [C₈C₁Im][BF₄] on ZnO (10 $\bar{1}$ 0), the spectrum has been fitted with four peaks at 190.6 eV, 191.8 eV, 192.9 eV and 194.3 eV. The peaks at 192.9 eV and 194.3 eV are assigned to B₂O₃ and [BF₄][−], respectively, as with the ZnO (0001) surface. We assign the intense peak at 191.8 eV to the B atom in the BF₃ environment in the carbene–borane adduct. This B atom has a negative charge, so it will be far more negative than the B atom in the [BF₄][−] anion; therefore, we expect a peak at a lower binding energy. The small peak at 190.6 eV is likely to arise from another decomposition product.

The O 1s spectra for [C₈C₁Im][BF₄] on ZnO (0001) and ZnO (10 $\bar{1}$ 0) are shown in Figure S4 and summarised in Table S2 of the Supporting Information. Both spectra are fitted with 3 peaks corresponding to oxygen atoms in the ZnO surface, surface hydroxyl groups (OH) and molecular adsorbed water (H₂O). This is discussed further in the SI.

In summary, the XPS data show a clear difference in the IL thin films that were deposited on the two ZnO surfaces, as illustrated by a schematic model in Figure 4. [C₈C₁Im][BF₄] adsorbs mostly intact on the ZnO (0001) surface at room temperature before being cooled to −150 °C for measurement. There is some dissociation of [BF₄][−] anions, resulting in boron atoms attaching to the oxygen atoms in the ZnO surface and forming B₂O₃. H₂O is present in the thin film, which may have adsorbed when the sample was cooled. OH groups are also present, which is typical for ZnO. The deposition of [C₈C₁Im][BF₄] on the ZnO (10 $\bar{1}$ 0) surface at −150 °C resulted in the appearance of more chemical environments in the XPS spectra. We propose that the high temperature of the IL evaporator for an extended period of time caused some conversion of [C₈C₁Im][BF₄] to a carbene–borane adduct, producing a flux of both the IL and adduct vapours, which stuck to the ZnO (10 $\bar{1}$ 0) surface at low temperature. The adduct does not stick to surfaces at room temperature due to its high vapour pressure, so the adduct was not visible in the spectra for the ZnO (0001) surface where deposition occurred at room temperature. Since the ZnO (10 $\bar{1}$ 0) surface was cooled prior to deposition, H₂O, CO and OH species were already present on the surface, and more H₂O is likely to have adsorbed with the IL/adduct film during deposition. As with the ZnO (0001) surface, there is dissociation of [BF₄][−] anions forming B₂O₃ at the surface. In this experiment, measurements were only taken at −150 °C. More information could be obtained from a film that is deposited at a low temperature and heated until the IL desorbs. The subsequent experiment at ASTRID2 synchrotron follows the evolution of an IL film deposited on ZnO (0001) as it is heated from −150 °C to 200 °C.

3.2. Adsorption and Desorption of [C₄C₁Im][BF₄] on Polar ZnO (0001)

A summary of fitted peaks and assignments for the temperature study of [C₄C₁Im][BF₄] on ZnO (0001) is shown in Table 2. The C 1s spectra at NE and GE for [C₄C₁Im][BF₄] on ZnO (0001) at −150 °C, −80 °C, room temperature (RT), 88 °C and 200 °C are shown in

Figure 5 (NE on left panel, GE on right panel). The inset on the right panel of Figure 5 shows the NE and GE spectra at each temperature overlaid to highlight differences upon heating (NE solid lines, GE dotted lines). The shape of the region should be similar to that of the analogous $[\text{C}_8\text{C}_1\text{Im}][\text{BF}_4]$, but because the $[\text{C}_4\text{C}_1\text{Im}]^+$ cation has a shorter alkyl chain, the lowest BE peak has a smaller relative intensity [29,38]. At $-150\text{ }^\circ\text{C}$, for both the NE and GE spectra, the C 1s spectra are fitted with four peaks at binding energies of 284.4 eV, 286.2 eV, 287.0 eV and 288.3 eV. The largest peak at 284.4 eV can be assigned to the alkyl chain of the IL (C1 in Figure 1b), in agreement with the literature [29,35]. The peak at 286.2 eV arises from carbon atoms bonded to a nitrogen atom, C2 and C3 in Figure 1b. The peak at 287.0 eV arises from the carbon atom between the two nitrogen atoms in the imidazolium ring, C4 in Figure 1b. There is a small peak at 288.3 eV, which is more intense at NE than GE. This indicates that the C species is beneath the IL layers rather than at the surface since the NE spectra are more sensitive to signals from deeper within the sample. This signal could be due to contaminant CO adsorbed at the IL/ZnO interface. The clean ZnO substrate was cooled to $-150\text{ }^\circ\text{C}$ prior to depositing IL, and CO tends to adsorb onto oxide surfaces at low temperatures ($< -120\text{ }^\circ\text{C}$) [39,40]. According to the structure of $[\text{C}_4\text{C}_1\text{Im}][\text{BF}_4]$, shown in Figure 1b, the ratio of the C1 peak to the C2+C3 peak should be 3:4, so we would expect the C2,3 peak to have a larger intensity in the C 1s spectrum. However, the spectra show that the C2,3 peak has a lower intensity than the C1 peak. Due to the short mean free path at this energy, the orientation of a big molecule can lead to attenuation of a lower part of the molecule relative to an upper part. Here, the ring part of the cation is attenuated by other parts of the IL (either the alkyl chain of the cation or the anion). If the deposited layer contained any carbene–borane adduct from the evaporator (discussed in the $[\text{C}_8\text{C}_1\text{Im}][\text{BF}_4]$ data, above), the C 1s spectrum would be largely similar, so it would be difficult to distinguish.

Table 2. Summary of fitted peaks for $[\text{C}_4\text{C}_1\text{Im}][\text{BF}_4]$ on ZnO (0001). For C 1s, N 1s, F 1s and B 1s, the fitted peaks at $-150\text{ }^\circ\text{C}$ are shown; for O 1s, the fitted peaks at room temperature are shown (since the O 1s spectra is dominated by adsorbed gaseous species at low temperatures). See SI for tables of peaks fitted at other temperatures.

Region	BE (eV) (± 0.1)	Assignment
C 1s (at $-150\text{ }^\circ\text{C}$)	284.4	C1 in Figure 1b
	286.2	C2 + C3 in Figure 1b
	287.0	C4 in Figure 1b
	288.3	CO (adsorbed from vacuum)
N 1s (at $-150\text{ }^\circ\text{C}$)	399.7	Beam damage/carbene–borane adduct
	400.8	Beam damage/carbene–borane adduct
	401.6	N atoms in $[\text{C}_4\text{C}_1\text{Im}]^+$ cation
F 1s (at $-150\text{ }^\circ\text{C}$)	682.7	Zn-F
	684.4	Decomposition/carbene–borane adduct
	685.4	F atoms in $[\text{BF}_4]^-$ anion
B 1s (at $-150\text{ }^\circ\text{C}$)	194.3	B atom in $[\text{BF}_4]^-$ anion
O 1s (at room temp)	529.1	O_2^- atoms in ZnO surface
	530.7	OH groups
	531.7	B_2O_3 (or residual H_2O)

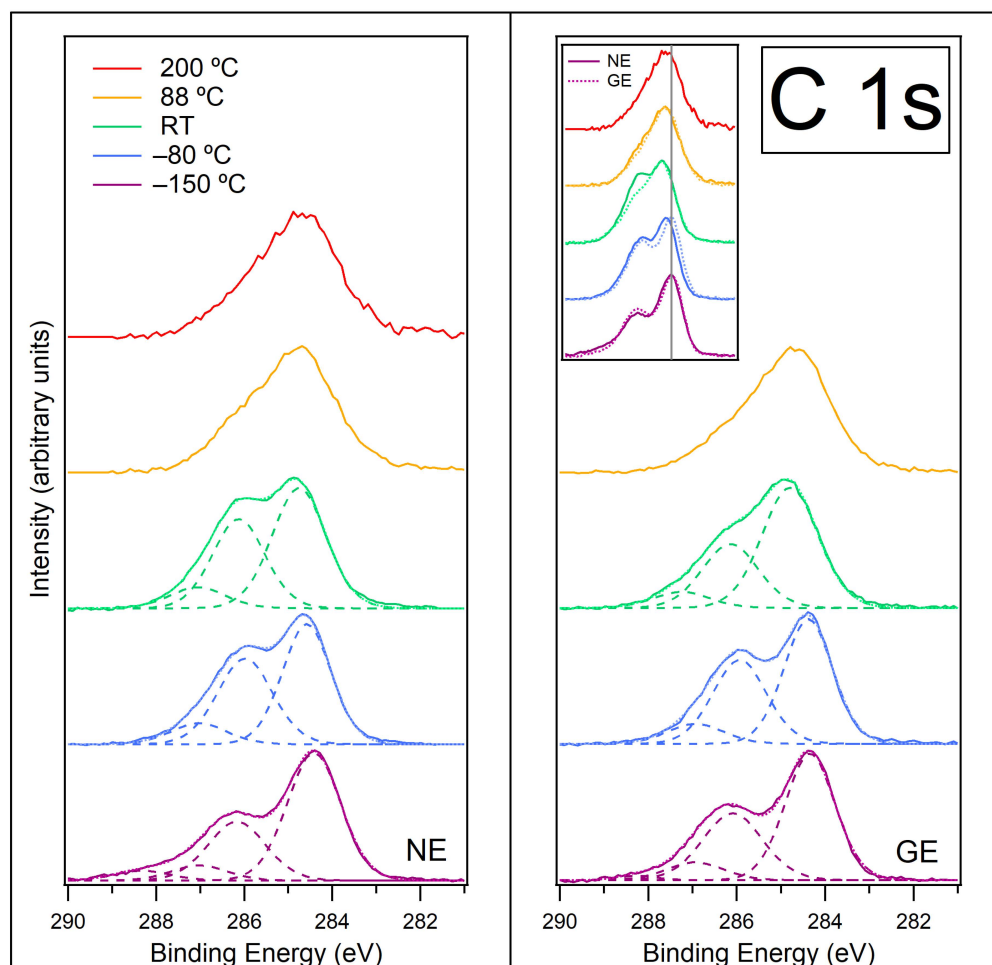


Figure 5. C 1s spectra recorded at normal emission NE (**left**) and at grazing emission GE (**right**) for $[\text{C}_4\text{C}_1\text{Im}][\text{BF}_4]$ on ZnO (0001) for temperatures $-150\text{ }^\circ\text{C}$, $-80\text{ }^\circ\text{C}$, room temperature (RT), $88\text{ }^\circ\text{C}$ and $200\text{ }^\circ\text{C}$. Components are fitted to the data at $-150\text{ }^\circ\text{C}$, $-80\text{ }^\circ\text{C}$ and RT. Fitted components are shown by dashed lines, and the resultant envelope is shown by a fainter dotted line. The inset on the right panel shows the C 1s spectra at NE (solid lines) and GE (dotted lines) overlaid to highlight the differences between them and to show the BE shifts upon heating (the grey line shows the position of the C1 environment at $-150\text{ }^\circ\text{C}$). The C 1s spectra have been normalised to the most intense feature at approximately 284.5 eV (C1 in Figure 1b). A photon energy of 370 eV was used to record this region.

Figure S5 in the SI shows the C 1s data at NE prior to normalisation. On heating the sample from $-150\text{ }^\circ\text{C}$ to $-80\text{ }^\circ\text{C}$, the intensity of the C 1s signal increases by over 2 times, implying more C species at the surface. This is consistent with the evaporation of water from the surface, leaving the $[\text{C}_4\text{C}_1\text{Im}]^+$ cations and $[\text{BF}_4]^-$ anions closer together and in contact with a stabilised water layer. At $-80\text{ }^\circ\text{C}$, the shoulder at 288.3 eV disappears for both NE and GE. This indicates that the CO has desorbed, presumably escaping through the IL layer to the vacuum. At $-80\text{ }^\circ\text{C}$, there is a shift to higher BE of the alkyl C1 peak at NE by approximately 0.2 eV (this shift can be seen clearly in the inset of Figure 5 by comparing the blue solid line (NE) to the blue dotted line (GE)). Table S3 in SI shows the BEs of fitted peaks as the sample is heated. This shift could be indicative of a phase transition of the IL from a glassy solid to a liquid and/or the change in interaction with the strongly bound, stabilised water layer. A phase transition to a liquid would allow any CO that was adsorbed at the ZnO surface to diffuse through. At this temperature, the ratio of the C1 peak to the C2,3+C4 peaks changes, with the C2,3+C4 peaks becoming relatively more intense. We propose that at $-150\text{ }^\circ\text{C}$, the $[\text{BF}_4]^-$ anion is located above the imidazolium rings and attenuates the C2,3+C4 signal, but by $-80\text{ }^\circ\text{C}$, the ions have moved, and the

imidazolium rings are located above the $[\text{BF}_4]^-$ ions, making the C2,3+C4 signal relatively larger. This indicates that the $[\text{BF}_4]^-$ ions preferentially move closer to the Zn^{2+} ions at the ZnO surface, possibly creating a layered $\text{Zn}^{2+}/[\text{BF}_4]^-/[\text{C}_4\text{C}_1\text{Im}]^+$ structure.

As the sample is heated to room temperature (RT), the C 1s signal decreases (Figure S5 in SI). This could indicate some desorption of IL from the surface, but this would be a very low temperature for IL to desorb. It is more likely that the IL is coalescing into islands on the surface as it becomes liquid. Islands are formed when the surface energy (surface tension) of the IL is greater than the interfacial energy between the IL and the ZnO surface and a balance is established. Several studies have shown that ionic liquids can form island structures on metal surfaces [41–44]. The islands have a smaller footprint on the surface than the layered structure, and since we are still probing the same depth of material, this gives a lower intensity signal. The presence of islands exposes parts of the ZnO surface. It is also likely that the adsorption of $[\text{C}_8\text{C}_1\text{Im}][\text{BF}_4]$ on ZnO (0001) at RT forms islands (ANTARES experiments, Figure 4), and these islands are frozen solid on cooling to $-150\text{ }^\circ\text{C}$ for analysis. At RT, the C1 peak shifts further to higher BE for both the NE and GE spectra, with the C1 peak now fitted at 284.8 eV for both spectra. The C2,3 peak remains at approximately the same BE. The BE separation between the alkyl peak and the C2,3 peak is reduced by $\sim 0.4\text{ eV}$ compared to the separation at $-150\text{ }^\circ\text{C}$. This is consistent with a major structural change on the surface, such as island formation. Similar changes in BE following a phase transition have previously been reported for an imidazolium-based IL on a metal surface [43]. At RT, there is a significant difference in the relative intensity of the C1 alkyl peak and the C2,3+C4 peaks between GE and NE, with the C1 peak being relatively more intense at GE. Since GE spectra are more surface-sensitive than NE spectra, this is indicative of a preferential orientation of the alkyl chains pointing out towards the vacuum with the ring part of the cation residing beneath it. This has been reported previously for this IL on various substrates [30–33].

As the sample is heated to $88\text{ }^\circ\text{C}$, the C 1s signal drops dramatically (Figure S5 in SI) as the IL desorbs from the surface, along with any carbene–borane adduct. There is a change in the shape of the C 1s region, which evolves from being composed of two distinct features to one asymmetrical feature with maximum intensity at $\sim 284.6\text{ eV}$. The shape of the spectra at GE and NE are similar. This indicates that the layered structure found at RT (alkyl chains towards vacuum, rings underneath) is no longer present and that some chemical changes have occurred in the remaining material, resulting in new carbon species on the surface. This change in the shape of the spectra suggests there are likely to be several decomposition species present on the surface; therefore, peaks have not been fitted to these spectra. Babucci et al. [45] demonstrated that $[\text{C}_4\text{C}_1\text{Im}][\text{BF}_4]$ in contact with ZnO powder decomposes when the system is kept at a constant temperature of $250\text{ }^\circ\text{C}$ for periods of 6, 10 and 24 h, resulting in higher levels of decomposition for the longer time periods. In our data, it appears that at $88\text{ }^\circ\text{C}$, we are already observing decomposition of $[\text{C}_4\text{C}_1\text{Im}][\text{BF}_4]$, which suggests the ZnO (0001) surface has a catalytic effect on the reaction.

As the surface is heated to $200\text{ }^\circ\text{C}$, there is a further decrease in intensity of the C 1s signal at NE (Figure S5 in SI), indicating that more material has desorbed from the surface. There is very little change in the shape of the C 1s spectrum at NE, suggesting that the chemical decomposition on the surface has finished. A possible decomposition mechanism for $[\text{C}_4\text{C}_1\text{Im}][\text{BF}_4]$ is C–N bond cleavage at either the methyl or butyl group attached to the imidazolium ring, which causes the IL to break down into a variety of hydrocarbon species [46]. Combined with decomposition of the anion, various alkylfluoride species (such as 2-propylfluoride and 1-fluorobutane) could also be formed [47]. However, any small molecules such as these would desorb at this high temperature and not be visible in the spectrum. The organic material remaining on the surface is likely to be polymeric

since it is relatively stable at 200 °C. The formation and desorption of such small molecules would explain the continued reduction in C 1s intensity whilst the polymerisation of the remaining surface occurs.

The N 1s spectra at NE and GE for $[\text{C}_4\text{C}_1\text{Im}][\text{BF}_4]$ on ZnO (0001) at -150 °C, -80 °C, room temperature (RT) and 88 °C are shown in Figure 6 (NE on left panel, GE on right panel). At -150 °C, the NE spectrum is fitted with three peaks at 399.7 eV, 400.8 eV and 401.6 eV (GE spectrum is fitted with three peaks at similar BEs; see Table S4 in SI for a summary of all fitted peaks). The most intense peak at 401.6 eV is attributed to nitrogen atoms in the $[\text{C}_4\text{C}_1\text{Im}]^+$ cation, which agrees with data presented for $[\text{C}_8\text{C}_1\text{Im}][\text{BF}_4]$ on ZnO (0001) and ZnO (10 $\bar{1}$ 0) and with the literature [29,35]. The other two peaks suggest that some decomposition of the IL may have occurred. The lower BE peaks are relatively more intense in the GE spectrum, suggesting these species reside in the top-most layers of the IL. Since the IL was deposited at -150 °C, thermal decomposition is unlikely. We suggest these lower BE peaks could arise from beam damage that occurred whilst taking measurements under the X-ray beam. It is also possible that one of these peaks may be due to the carbene–borane adduct adsorbed from the evaporator.

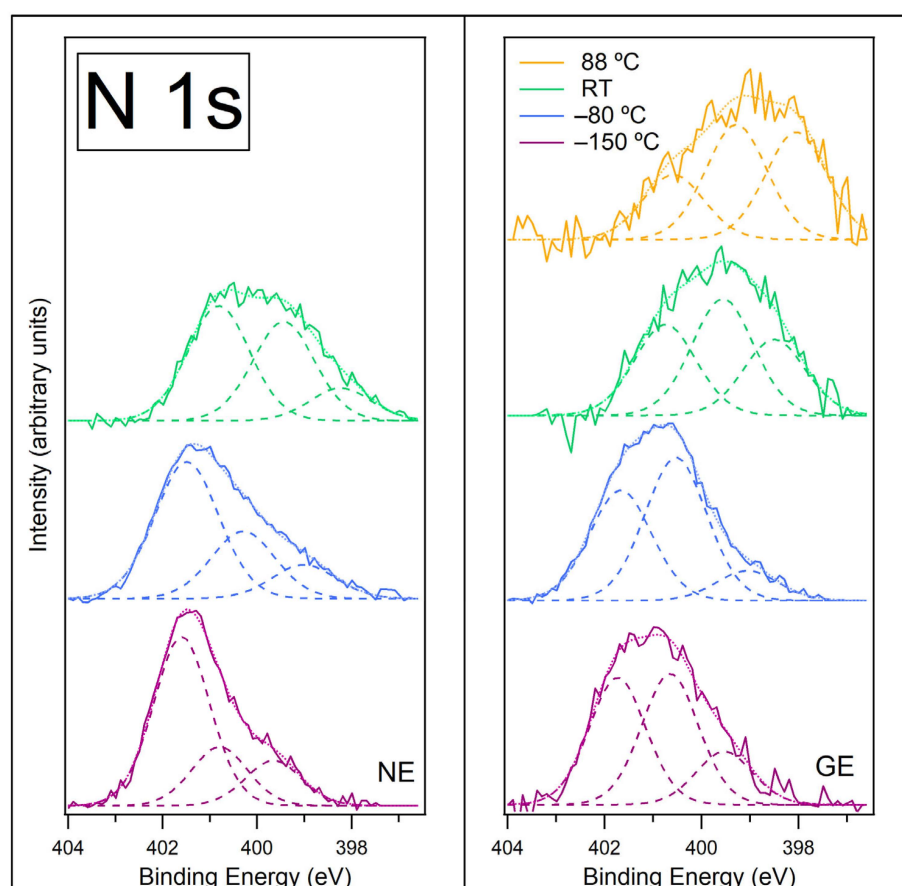


Figure 6. N 1s spectra recorded at normal emission NE (left) and at grazing emission GE (right) for $[\text{C}_4\text{C}_1\text{Im}][\text{BF}_4]$ on ZnO (0001) for temperatures -150 °C, -80 °C, room temperature (RT) and 88 °C. Fitted components are shown by dashed lines, and the resultant envelope is shown by a fainter dotted line. The N 1s spectra have been normalised to the total area of the region. A photon energy of 480 eV was used to record this region.

Figure S6 in the SI shows the N 1s data at GE prior to normalisation. On heating from -150 °C to -80 °C, the intensity of the N 1s signal increases by over 2 times, implying more N species at the surface. This is consistent with the evaporation of water from the surface, leaving the $[\text{C}_4\text{C}_1\text{Im}]^+$ cations and $[\text{BF}_4]^-$ anions closer together and in contact

with a stabilised water layer. At $-80\text{ }^{\circ}\text{C}$, the shape of the spectra remains similar, but the lower BE peaks become relatively more intense. As with the $-150\text{ }^{\circ}\text{C}$ data, the lower BE peaks are relatively more intense in the GE spectrum, suggesting these species reside in the top-most layers of the IL. The increase in intensity of the lower BE peaks could be indicative of further beam damage, or this could be due to beam damage that was previously frozen in position throughout the layer at $-150\text{ }^{\circ}\text{C}$, now diffusing upward to the surface as the IL starts to melt. The peak assigned to N atoms in the $[\text{C}_4\text{C}_1\text{Im}]^+$ cation is still fitted at the same BE; however, the lower BE peaks have shifted to lower BEs. The shifts in BE could coincide with a phase transition of the IL from a glassy solid to a liquid and/or the change in interaction with the strongly bound stabilised water layer. If one of these lower BE peaks is the adduct, then the shift could be due to the change in chemical environment as most of the water desorbs.

As the sample is heated to room temperature (RT), the N 1s signal decreases significantly (by $\sim 73\%$ of its intensity at $-80\text{ }^{\circ}\text{C}$, Figure S6 in SI), as observed with the C 1s signal. The spectra also change shape, with lower BE peaks becoming more prominent. This is consistent with the formation of islands on the surface, leaving large areas between the droplets covered in beam damage products. The spectra are difficult to fit with any certainty, but it appears that the peak assigned to N atoms in the $[\text{C}_4\text{C}_1\text{Im}]^+$ cation at approximately 401.6 eV has shifted to 400.8 eV. This BE shift could be due to the IL going through a phase change and forming islands. The three peaks are now fit at 398.2 eV, 399.4 eV and 400.8 eV (at NE).

Heating to $88\text{ }^{\circ}\text{C}$ (only recorded for GE) causes the N 1s signal to decrease further (a decrease of $\sim 23\%$ of its intensity at RT, Figure S6 in SI), indicating the desorption of the IL islands and any carbene–borane adduct. The spectrum is shifted to even lower BEs, suggesting there is very little/no IL cation left on the surface. This leaves the ZnO surface covered with degradation products, which are likely to be polymeric. The small change in the N 1s intensity upon heating to $88\text{ }^{\circ}\text{C}$ indicates that the small footprint of the IL islands has little effect on the signal when removed, so the changes observed in the spectrum are primarily changes to the degradation products that cover most of the surface.

The F 1s spectra at NE and GE for $[\text{C}_4\text{C}_1\text{Im}][\text{BF}_4]$ on ZnO (0001) at $-150\text{ }^{\circ}\text{C}$, $-80\text{ }^{\circ}\text{C}$, room temperature (RT), $88\text{ }^{\circ}\text{C}$ and $200\text{ }^{\circ}\text{C}$ are shown in Figure 7 (NE on left panel, GE on right panel). At $-150\text{ }^{\circ}\text{C}$, the NE spectrum is fitted with three peaks at 682.7 eV, 684.4 eV and 685.4 eV (GE spectrum is fitted with three peaks at similar BEs; see Table S5 in SI for a summary of all fitted peaks). The main feature of the spectrum (centred at $\sim 684.7\text{ eV}$) looks symmetrical, so one might be inclined to fit just one peak here. However, the full width half maximum (FWHM) of this feature is rather broad, so to be consistent with the FWHM of peaks fitted to other regions, it requires more than one fitted peak. The peaks fit to the C 1s spectrum at $-150\text{ }^{\circ}\text{C}$ (where the peak at 285 eV is very clearly defined) have a FWHM of $\sim 1.5\text{ eV}$, and this is the typical FWHM across the different regions. The three fitted F 1s peaks shown in Figure 7 have a FWHM of $\sim 1.7\text{ eV}$, which is slightly larger than the FWHM across other regions but seems appropriate to avoid “over-fitting” the spectrum with more peaks. The peak at 685.4 eV is assigned to F atoms in the $[\text{BF}_4]^-$ anion [29], in reasonable agreement with data presented for $[\text{C}_8\text{C}_1\text{Im}][\text{BF}_4]$ on ZnO (0001) in the ANTARES experiment. We believe the $[\text{BF}_4]^-$ ions reside in a water layer near the surface of the IL (evidence for this is presented in the B 1s discussion). We assign the peak at 684.4 eV to a decomposition product and/or from the carbene–borane adduct adsorbed from the evaporator. The smallest peak at 682.7 eV is lower in BE than any peaks fit in the ANTARES experiment and on the lower edge of F 1s BEs in the literature. We propose this could be due to a Zn–F bond at the ZnO surface, although the values in the literature for Zn–F are usually found at higher BEs than this.

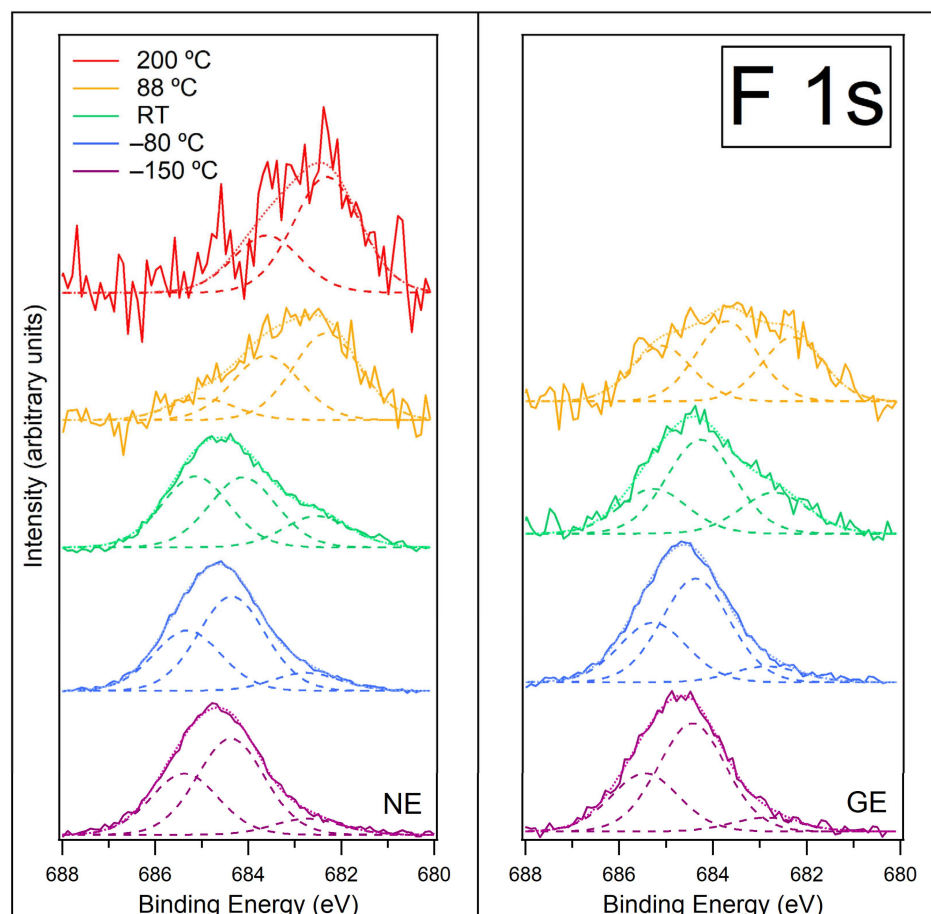


Figure 7. F 1s spectra recorded at normal emission NE (**left**) and grazing emission GE (**right**) for $[\text{C}_4\text{C}_1\text{Im}][\text{BF}_4]$ on ZnO (0001) for temperatures $-150\text{ }^\circ\text{C}$, $-80\text{ }^\circ\text{C}$, room temperature (RT), $88\text{ }^\circ\text{C}$ and $200\text{ }^\circ\text{C}$. Fitted components are shown by dashed lines, and the resultant envelope is shown by a fainter dotted line. The F 1s spectra have been normalised to the total area of the region. A photon energy of 770 eV was used to record this region.

Figure S7 in the SI shows the F 1s data at NE prior to normalisation. On heating from $-150\text{ }^\circ\text{C}$ to $-80\text{ }^\circ\text{C}$, the intensity of the F 1s signal increases, implying more F species at the surface. This is consistent with the evaporation of water from the surface, leaving the $[\text{C}_4\text{C}_1\text{Im}]^+$ cations and $[\text{BF}_4]^-$ anions closer together and in contact with a stabilised water layer. At $-80\text{ }^\circ\text{C}$, the shape of the spectra at NE and GE remain similar, and the same three peaks are fitted to both spectra at similar BEs. This indicates there is very little change in the chemical environments of the F atoms upon heating to this temperature.

As the sample is heated to room temperature (RT), the F 1s signal decreases significantly (by $\sim 55\%$ of its intensity at $-80\text{ }^\circ\text{C}$, Figure S7 in SI), indicating the formation of islands on the surface. The F 1s peak broadens, which could be caused by the IL going through a phase change and forming islands. The F 1s signal decreases by $\sim 55\%$ upon heating to RT, whereas the N 1s signal decreases by about $\sim 73\%$. This might indicate that island formation is less effective for the F-containing species at RT than it is for the N-containing cation. It is likely the decomposition species/carbene–borane adduct do not form islands and instead they spread out over the surface and lie between the islands of IL. Three peaks are still fitted to both the NE and GE spectra, but now, the lowest BE peak, assigned to a Zn-F bond at the ZnO surface, becomes relatively more intense. This is consistent with the formation of IL islands on the surface, leaving large areas between the droplets covered in Zn-F.

Heating to 88 °C causes the F 1s signal to drop again (a decrease of ~83% of its intensity at RT, Figure S7 in SI), indicating the desorption of the IL islands and any carbene–borane adduct. There is very little F remaining on the surface at this temperature. The spectrum changes shape, with the lower BE peaks becoming dominant. Further heating to 200 °C causes the F 1s signal to reduce slightly again (Figure S7 in SI). The peak at 685.4 eV due to F atoms in the $[\text{BF}_4]^-$ anion has completely disappeared, indicating that only decomposition products remain on the surface. The peak assigned to Zn-F at the ZnO surface is now the most intense peak. Numerous fluorine-containing species can be formed from the thermal decomposition of $[\text{C}_4\text{C}_1\text{Im}][\text{BF}_4]$ [46,47]; however, these small molecules would desorb at high temperatures and not contribute to the spectrum. It is difficult to identify what the remaining decomposition species might be.

The B 1s spectra at NE and GE for $[\text{C}_4\text{C}_1\text{Im}][\text{BF}_4]$ on ZnO (0001) at -150 °C, -80 °C, room temperature (RT), 88 °C and 200 °C are shown in Figure 8 (NE on left panel, GE on right panel). Large shifts in BE upon heating caused problems with spectra drifting outside the BE measurement window, and as a result, some spectra were slightly truncated. At -150 °C, both spectra are fitted with one peak at 194.3 eV, consistent with B atoms in the $[\text{BF}_4]^-$ anions [29] and consistent with data presented for $[\text{C}_8\text{C}_1\text{Im}][\text{BF}_4]$ on ZnO (0001). The N 1s and F 1s spectra both show clear signs of degradation/beam damage at -150 °C, but the B 1s spectrum does not. The F 1s spectrum is fitted with three chemical environments, so if the $[\text{BF}_4]^-$ anions have dissociated to form different F species, one would expect the B 1s spectrum to reflect this. However, if the $[\text{BF}_4]^-$ ions reside in a frozen water layer near the surface of the IL, the XPS spectrum is likely to be dominated by a strong signal from the $[\text{BF}_4]^-$ ions. There may be other B species throughout the depth of the adlayer, but since the photoelectron energy is low (and therefore very surface-sensitive), we do not detect the buried decomposition material, or alternatively, the BE of these species is very similar to the BE for $[\text{BF}_4]^-$.

Figure S8 in the SI shows the B 1s data at NE prior to normalisation. On heating from -150 °C to -80 °C, the intensity of the B 1s signal decreases, in contrast to the C 1s, N 1s and F 1s signals, which increased when heated to -80 °C. This suggests that at -150 °C, the B atoms were not attenuated by adsorbed water and were located near the vacuum interface. We propose that at -150 °C, the $[\text{BF}_4]^-$ anions could reside in a frozen water layer near the surface, giving a relatively stronger intensity. This would involve some of the $[\text{BF}_4]^-$ anions moving away from the $[\text{C}_4\text{C}_1\text{Im}]^+$ cations. This would be a solid-state version of dissolving the IL in water, where each ion moves away from the opposite ion and becomes hydrated. The ions do not have to move far, and the activation energy for diffusion is much lower than chemical reaction, so the $[\text{BF}_4]^-$ anions can move even at -150 °C. $[\text{BF}_4]^-$ anions that are still associated with $[\text{C}_4\text{C}_1\text{Im}]^+$ cations may also contribute to the single fitted peak at -150 °C, as the change in environment from $[\text{C}_4\text{C}_1\text{Im}]^+$ to H_2O is unlikely to affect the B chemical shift in $[\text{BF}_4]^-$. Upon heating to -80 °C, the decrease in intensity is caused by a rearrangement of the ions, implying some $[\text{BF}_4]^-$ ions have moved deeper into the adlayer. At this temperature, most of the water has desorbed, and the remaining water is associated with both ions of the IL, forming a stabilised water layer. At -80 °C, the spectra at NE and GE shift slightly to lower BE and become broader towards lower BE. Both spectra are fitted with two peaks at approximately 193.3 eV and 194.2 eV (see Table S6 in SI for a summary of all fitted peaks). We assign the peak at 194.2 eV to B atoms in the $[\text{BF}_4]^-$ anion. The peak at 193.3 eV suggests some decomposition on the surface. The peak at 193.3 eV is relatively more intense in the NE spectra than for the GE spectra, which suggests that this species is more prevalent deeper in the adlayer, closer to the ZnO substrate, rather than at the surface of the IL. This could be a decomposition product, or it could be due to BF_3^- in the carbene–borane adduct, which would have a

lower BE than $[\text{BF}_4]^-$. If this is due to the adduct (adsorbed from the evaporator with the IL), then the adduct would have mixed with the IL and been overlaid with water. Heating to -80°C causes a rearrangement in the adlayer, so the adduct could diffuse towards the surface and become more visible. Interestingly, the F 1s spectra showed very little change upon heating from -150°C to -80°C , so it is not clear what change is occurring or why the F 1s intensity changes do not match the changes observed for the B 1s.

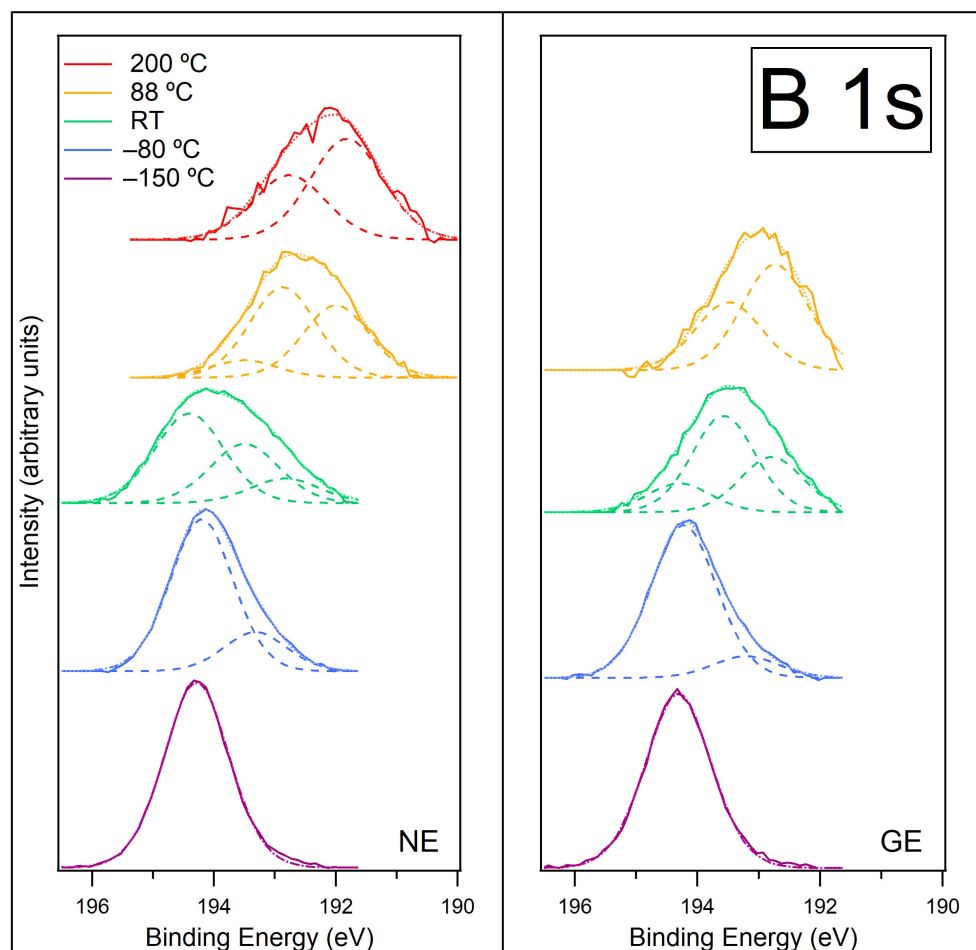


Figure 8. B 1s spectra recorded at normal emission NE (left) and at grazing emission GE (right) for $[\text{C}_4\text{C}_1\text{Im}][\text{BF}_4]$ on ZnO (0001) for temperatures -150°C , -80°C , room temperature (RT), 88°C and 200°C . Fitted components are shown by dashed lines, and the resultant envelope is shown by a fainter dotted line. The B 1s spectra have been normalised to the total area of the region. A photon energy of 270 eV was used to record this region.

As the surface is heated to room temperature (RT), the B 1s signal decreases significantly (by $\sim 47\%$ of its intensity at -80°C , Figure S8 in SI), in agreement with the decrease observed in the C 1s, N 1s and F 1s signals, indicating the formation of islands on the surface. The % decrease in the B 1s signal is very similar to that seen with the F 1s signal (and much less than the decrease in the N 1s signal), indicating that decomposition species/carbene–borane adducts spread out over the surface and lie between the islands of IL. The spectra broaden further, and three peaks are now required to fit both NE and GE spectra, at approximately 192.8 eV, 193.5 eV and 194.4 eV. The additional peak at 192.8 eV is consistent with the BE of B atoms in a B_2O_3 environment [37], as we previously assigned for $[\text{C}_8\text{C}_1\text{Im}][\text{BF}_4]$ on the ZnO (0001) and ZnO (10 $\bar{1}$ 0) surfaces. This could arise from dissociation of the $[\text{BF}_4]^-$ anions where B atoms attach to the O atoms at step edges in the ZnO (0001) surface. The reaction between the ZnO surface and $[\text{BF}_4]^-$ produces B_2O_3

and fluorine-containing species, which might be organic or might react with the surface to form Zn-F. The peaks at 194.4 eV and 193.5 eV are again assigned to the $[\text{BF}_4]^-$ anion and decomposition/adduct, respectively. The peak at 193.5 eV is more intense at GE, indicating that this species is nearer the surface of the adlayer. If it is the adduct, it may be mixed with the IL and/or between the islands.

Further heating to 88 °C causes the B 1s signal to reduce further (Figure S8 in SI), indicating the desorption of the IL islands and any carbene–borane adduct. The spectra change shape and shift to lower binding energy. At 88 °C, the component previously assigned to $[\text{BF}_4]^-$ (at ~194.4 eV) has completely disappeared, and the peak attributed to decomposition/adduct is reduced in intensity. This indicates that the IL and the adduct have both evaporated from the surface on heating to 88 °C. The peak at ~192.8 eV due to B_2O_3 is relatively more intense. This is most likely due to the removal of the IL overlayer, although some further reaction to produce B_2O_3 may have occurred during heating. A new peak at 192 eV is now visible, which is not easy to identify but is likely to be a decomposition product.

Further heating to 200 °C causes the B 1s signal to reduce further again (Figure S8 in SI), indicating further desorption of material from the surface. The spectrum is fitted with two peaks at 191.8 eV and 192.8 eV, assigned to decomposition and B_2O_3 , respectively.

The most significant changes in the C 1s, N 1s, F 1s and B 1s spectra occur as the surface is heated from room temperature to 88 °C. At 88 °C, all spectra show a reduction in intensity, indicating the desorption of the IL islands and any carbene–borane adduct. The B and F spectra are consistent in showing that the $[\text{BF}_4]^-$ anion of the IL has mostly/completely disappeared at 88 °C. At 88 °C, peaks assigned to degradation products and reactions at the ZnO surface become relatively more intense, indicating that the ZnO surface may catalyse the thermal decomposition of the IL at low temperature.

The O 1s spectra at NE and GE for $[\text{C}_4\text{C}_1\text{Im}][\text{BF}_4]$ on ZnO (0001) at –150 °C, –80 °C, room temperature (RT), 88 °C and 200 °C are shown in Figure 9 (NE on left panel, GE on right panel). The spectra at –150 °C and –80 °C are very broad due to several species adsorbing to the surface at low temperatures; therefore, these spectra have not been fitted with peaks.

There are two broad features visible at –150 °C: a large feature at approximately 532.5 eV and a smaller feature at approximately 529 eV. The feature at ~529 eV is assigned to O atoms in the ZnO substrate [24,48,49]. The signal from the ZnO substrate is clearly visible at NE, but the signal is very weak at GE because this measurement does not probe as deep into the adlayer. The feature at ~532.5 eV spans a large BE range and is assigned to overlapping peaks from water and other contaminants, which have condensed onto the surface from the background vacuum during cooling [50,51]. The width of this feature makes peak fitting difficult, and it is not clear from the data if the water and other contaminants are located on top of the IL or mixed with the IL. Adsorbed water may be in a variety of chemical states where it is frozen in contact with the $[\text{C}_4\text{C}_1\text{Im}]^+$ or $[\text{BF}_4]^-$ ions in different geometries. This range of different chemical environments will broaden the 532.5 eV feature. We would expect hydroxyl (OH) groups to be present at the ZnO surface, which tend to manifest in the O 1s spectrum at binding energies ~1.4 eV–1.6 eV greater than the substrate O [48–50,52]. However, these are unlikely to contribute much to the 532.5 eV feature as they are low in concentration, and their signal will be attenuated by the overlayer of IL and water (the ZnO signal at 529 eV is very small so the signal from the OH groups attached to the ZnO surface will be tiny). We also expect CO to be adsorbed on the ZnO surface, which typically appears at higher BEs in O 1s spectra [53–55]. However, this is also unlikely to contribute much to the 532.5 eV feature because its signal will be attenuated by the overlayer, as with the OH groups. The discussion for the O 1s region of $[\text{C}_8\text{C}_1\text{Im}][\text{BF}_4]$ on ZnO (0001) and ZnO (10 $\bar{1}$ 0) (see SI, Figure S4 and discussion

thereof) goes into further details about O 1s assignments. If the IL was deposited at room temperature instead of $-150\text{ }^{\circ}\text{C}$, this would largely eliminate the adsorption of water and other contaminants between the IL layers and would make an interesting comparison to this study.

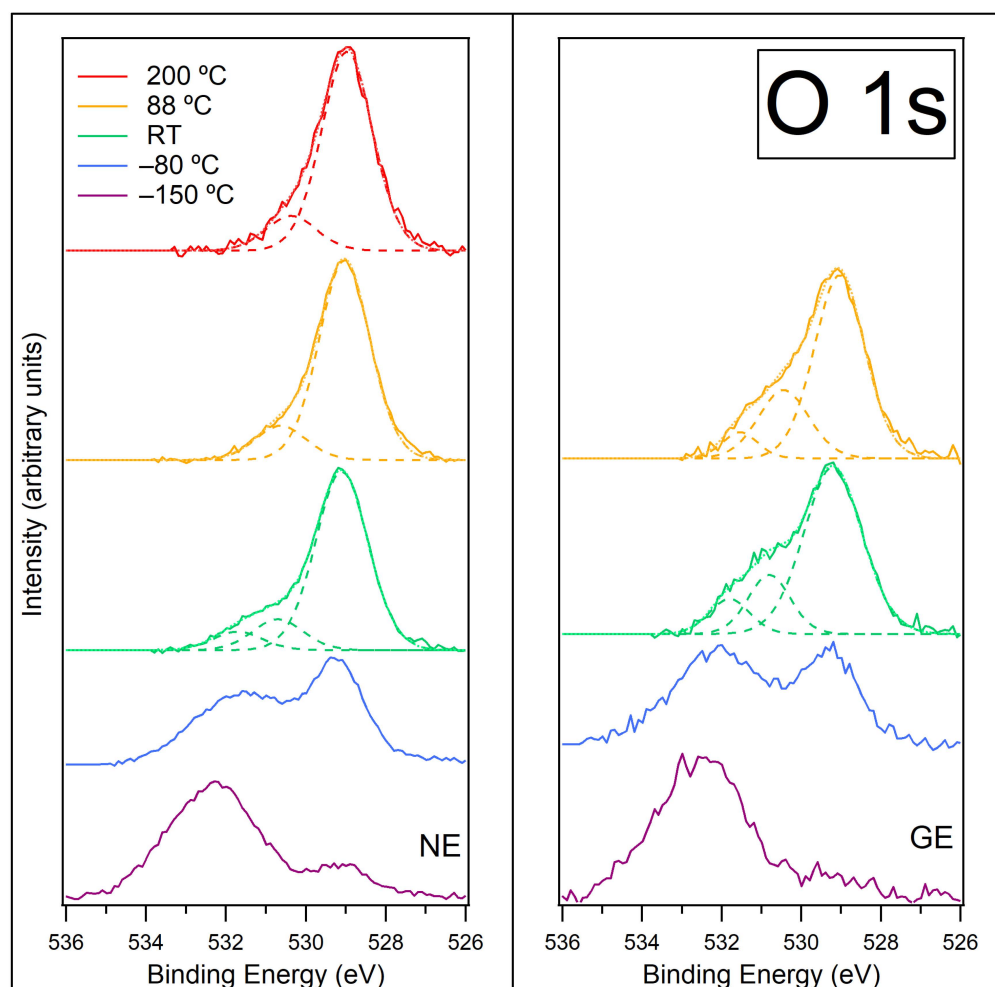


Figure 9. O 1s spectra recorded at normal emission NE (**left**) and grazing emission GE (**right**) for $[\text{C}_4\text{C}_1\text{Im}][\text{BF}_4]$ on ZnO (0001) for temperatures $-150\text{ }^{\circ}\text{C}$, $-80\text{ }^{\circ}\text{C}$, room temperature (RT), $88\text{ }^{\circ}\text{C}$ and $200\text{ }^{\circ}\text{C}$. Components are fitted to the data at RT, $88\text{ }^{\circ}\text{C}$ and $200\text{ }^{\circ}\text{C}$. Fitted components are shown by dashed lines, and the resultant envelope is shown by a fainter dotted line. The O 1s spectra have been normalised to the total area of the region. A photon energy of 610 eV was used to record this region.

Figure S9 in the SI shows the O 1s data at NE prior to normalisation. On heating from $-150\text{ }^{\circ}\text{C}$ to $-80\text{ }^{\circ}\text{C}$, the feature at $\sim 532.5\text{ eV}$ decreases in relative intensity while the feature at $\sim 529\text{ eV}$ increases in relative intensity. This is due to adsorbed gaseous species desorbing from the surface and O atoms in the ZnO surface becoming more prominent (as they become less attenuated by adsorbed species). This supports the theory of desorption of CO from the ZnO surface as indicated by the C 1s spectrum at $-80\text{ }^{\circ}\text{C}$. Water multilayers are likely to desorb at this temperature, and this will be the main cause of the changes observed in the O 1s spectra [51,56]. The absolute intensity of the feature at 532.5 eV is similar to its absolute intensity at $-150\text{ }^{\circ}\text{C}$ (Figure S9 in SI), but it is now shifted to a lower BE. We propose the remaining water is associated with the IL but is now better ordered to the ions, such that the average BE is now lower. Similar behaviour has been previously observed where multilayers of water were found to desorb from an imidazolium-based IL at approximately $-90\text{ }^{\circ}\text{C}$ and left a residual monolayer that did not desorb until approximately $-30\text{ }^{\circ}\text{C}$ [56]. At GE, the high binding energy feature is relatively more intense (compared to the ZnO

peak) and more defined, which is consistent with the associated water being more abundant in the topmost layers of the IL. It is still unlikely that OH groups or CO will contribute much to the O 1s spectrum at this temperature due to the attenuating overlayer.

As the sample is heated to room temperature (RT), the O 1s signal from the ZnO surface increases further, and the O 1s signal from the adsorbed gaseous species decreases further (Figure S9 in SI). It now becomes feasible to fit three peaks to the spectra (shown in Figure 9). The dominant peak at a binding energy of 529.1 eV is assigned to O atoms in the ZnO substrate, and the peak at 530.7 eV is assigned to OH groups. The peak at 531.7 eV could be due to residual H₂O and/or B₂O₃ [57] (which appeared in the B 1s spectra at RT). The water associated with the IL ions will now be desorbed, so the intensity of the ZnO peak increases as there is less attenuation from the adlayer. In addition, the IL forms islands on the surface at room temperature, which exposes areas of the ZnO substrate. This contributes to the large increase in intensity of the ZnO peak. The formation of islands also exposes the OH groups and B₂O₃, which are adsorbed to the ZnO surface, and they can now be seen in the spectrum as they are no longer attenuated by the overlayer. If any residual H₂O does exist, this could be associated with the ZnO/IL interface, giving a particularly high desorption energy. The OH and B₂O₃/H₂O peaks have a higher relative intensity at GE than at NE, indicating that these species are predominantly present at the shallower probing depth. It is not clear why this would be the case. If the probing depth at GE (~1.0 nm) closely matches the thickness of the film at this temperature, these species might give a relatively more intense peak than at NE, where more of the ZnO substrate is probed.

On heating to 88 °C, the intensity of the signal from the ZnO surface does not change. The IL islands have mostly evaporated from the surface at 88 °C, so the islands must have occupied a small area on the surface for the ZnO intensity to remain unchanged. The signal from the higher BE peaks is reduced further (Figure S9 in SI). At NE, the peak at 531.7 eV assigned to B₂O₃/H₂O has gone, and the peak assigned to OH has reduced; however, both peaks still remain at GE (Figure 9). Small amounts of water in ILs are usually removed by heating to ~60–80 °C under UHV [58,59], so it is likely the peak at 531.7 eV is now only due to B₂O₃.

On heating to 200 °C, the C, N, F and B peaks all drop to low intensities, indicating that almost the entire adlayer has desorbed. However, the O peak due to the ZnO substrate also drops to about 1/3 of its value at 88 °C (Figure S9 in SI). This cannot be due to attenuation of the signal, as there is almost no material to attenuate the ZnO substrate. Instead, it must be due to a loss of oxygen from the ZnO surface within a mean free path depth. Batyrev et al. studied the ZnO (0001)–Zn terminated surface after reduction at various temperatures using a combination of surface science techniques [15]. They exposed the clean ZnO surface to 1×10^{-5} mbar H₂ at temperatures up to 900 K. They found that the electronic structure changed from an n-type semiconductor towards a semi-metallic character. At 227 °C, the subsurface of the ZnO is n-type but with metallic surface states. The authors believe the metallisation of the surface occurred from the reduction of ZnO to metallic Zn and OH. The authors recorded O 1s XPS after reduction in 1 bar H₂ at RT, and this showed a decrease in the intensity of the ZnO substrate peak and an increase in the OH peak. In our study, we did not expose the ZnO surface to H₂ gas, but the decomposed adlayer at 88 °C contained H, C, N, F and B. It is conceivable that O²⁻ from the ZnO surface could react with the adlayer at high temperature to form H₂O, CO and NO, and all three would desorb, leaving a Zn rich surface. Batyrev et al. proposed that the net effect of OH formation during reduction and the removal of water during annealing caused 25% of the ZnO surface to reduce to metallic Zn [15]. In our O 1s spectra, there is a reduction in the ZnO substrate intensity by 2/3 upon heating from 88 °C to 200 °C, which could be caused by the loss of O atoms

from the surface region. The O 1s spectra at 200 °C are still fitted with a small peak at a higher BE, which could be the remaining B₂O₃. A schematic model showing the proposed behaviour of [C₄C₁Im][BF₄] on ZnO (0001) as the sample is heated is shown in Figure 10.

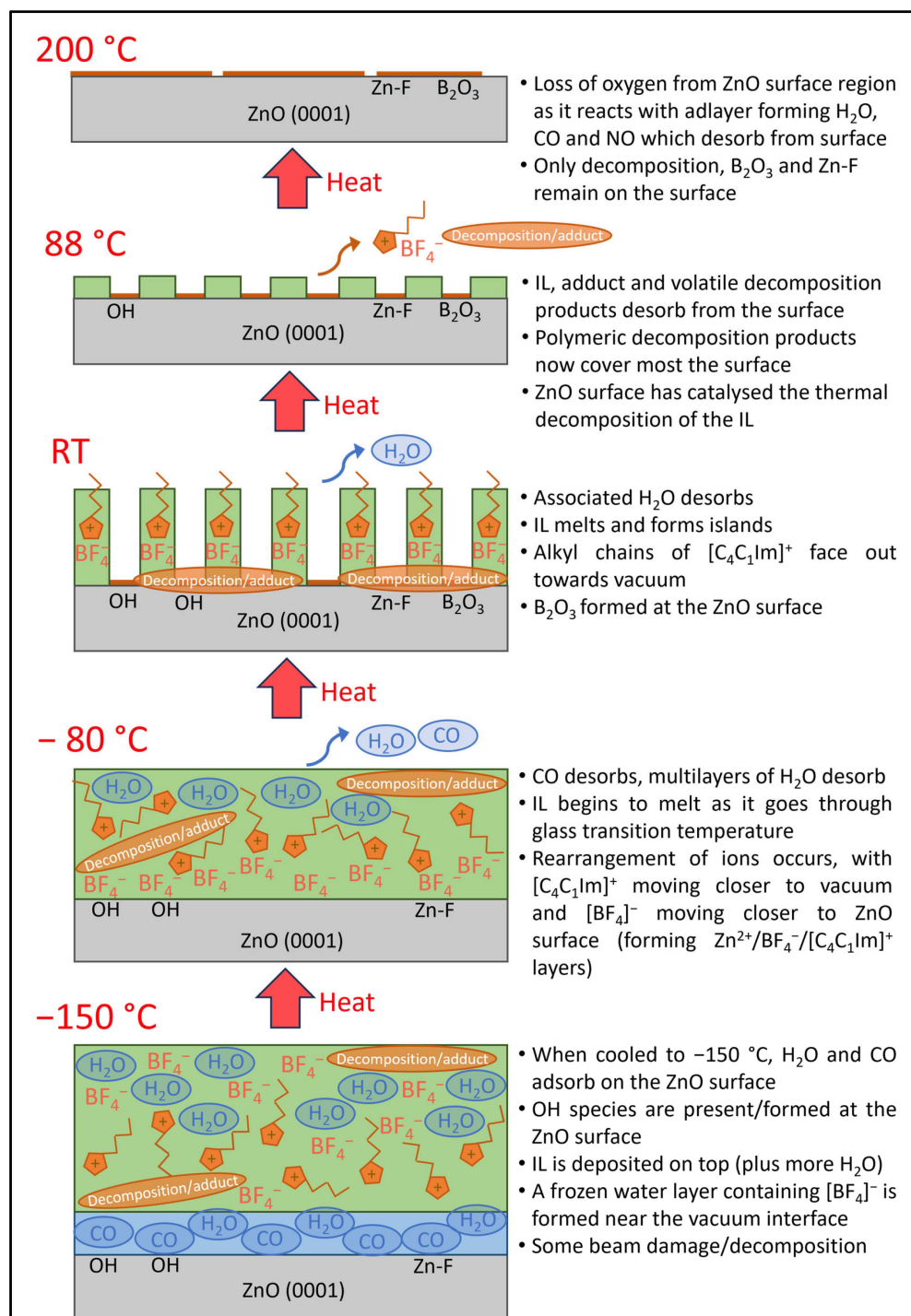


Figure 10. A schematic model showing the proposed behaviour of [C₄C₁Im][BF₄] on ZnO (0001) as the sample is heated from -150 °C to 200 °C.

4. Discussion

Many of the early studies into the decomposition of ILs used fast-scanning thermogravimetric analysis TGA to determine the temperature of onset of decomposition. These methods involved a fast ramp-up in temperature (in excess of 10 °C/min), heating the ILs to high temperatures for relatively short periods of time [26,60–62]. Therefore, the tempera-

tures at which ILs decompose in those conditions are sometimes referred to in the literature as the onset temperature, or T_{onset} [63]. This value is seen as an overestimate of their thermal stability in the context of heat-transfer applications, where ILs can undergo significant decomposition if they are exposed to lower temperatures than their onset temperature but for extended periods of time. This phenomenon is referred to as long-term thermal stability. The long-term thermal stability of an IL will change depending on the desired working temperature, and the time for which the IL is kept at that temperature [61,64,65]. One property often reported to quantify the long-term thermal stability of ILs is $T_{0.01/10\text{h}}$. It is defined as the temperature at which 1% of the IL mass is lost over a period of 10 h. Studies into the long-term thermal stability of 1-alkyl-*n*-imidazolium tetrafluoroborate ILs have reported a significant difference between T_{onset} and $T_{0.01/10\text{h}}$ but are still considered very thermally stable since both temperature values are high. Cao et al. [66] found that for $[\text{C}_8\text{C}_1\text{Im}][\text{BF}_4]$, $T_{0.01/10\text{h}}$ was 199 °C and T_{onset} was 397 °C, giving a difference of 198 °C between the two values. For the purposes of physical vapour deposition (PVD) in UHV, the IL is heated to an appropriate temperature between $T_{0.01/10\text{h}}$ and T_{onset} (this will also depend on the pressure in the chamber). When the IL vaporises, it is carried through the pressure gradient and deposited as ion pairs on the substrate [67,68]. The IL should not be heated to such a temperature that it begins to decompose.

As mentioned earlier in the manuscript, a study into reactive distillation of ILs [34] showed that refluxing $[\text{C}_4\text{C}_1\text{Im}][\text{BF}_4]$ under vacuum for extended periods of time resulted in the formation of a carbene–borane adduct, in which the acidic H on the imidazole was replaced by BF_3 to produce 1-butyl-3-methylimidazolium-2-trifluoroborate with elimination of HF. $[\text{C}_8\text{C}_1\text{Im}][\text{BF}_4]$ was also studied, and a similar carbene–borane adduct was produced: 1-octyl-3-methylimidazolium-2-trifluoroborate. For our deposition of $[\text{C}_8\text{C}_1\text{Im}][\text{BF}_4]$ on ZnO (0001), the IL was heated with a rate of ~ 22 °C/min to ~ 350 °C prior to deposition and was held at this temperature for ~ 20 min (however, the thermocouple was in contact with the metal shell of the evaporator, not the IL itself, so we expect the real temperature of the IL to be lower than this). For ZnO (10 $\bar{1}$ 0), the deposition temperature was the same, but the deposition time was ~ 420 min. Being held at this temperature for long periods of time may have caused formation of the carbene–borane adduct in the evaporator; therefore, both the IL and adduct would impinge on the ZnO surface during deposition. Since the ZnO (10 $\bar{1}$ 0) surface was at -150 °C during deposition, it is more likely the adduct would stick to the surface, whereas the ZnO (0001) surface was at room temperature during deposition, where the adduct is less likely to stick to the surface (the adduct has a higher vapour pressure than the IL). The differences observed in the XPS spectra are consistent with the adduct being present on the ZnO (10 $\bar{1}$ 0) surface but not on the ZnO (0001) surface.

In the adsorption and desorption study of $[\text{C}_4\text{C}_1\text{Im}][\text{BF}_4]$ on polar ZnO (0001), we observed the decomposition of the IL at 88 °C, which suggests the ZnO (0001) surface has a catalytic effect on the reaction. The polar ZnO (0001) surface has previously been shown to catalyse the decomposition of small molecules such as methanol and formic acid [69,70] and ZnO-based catalysts are commonly used in methanol synthesis [71]. Babucci et al. [45] showed that the thermal stability limits of ILs are significantly reduced when deposited on powdered ZnO. They investigated the short-term thermal stability limits of $[\text{C}_4\text{C}_1\text{Im}][\text{BF}_4]$ on powdered ZnO compared to values for bulk $[\text{C}_4\text{C}_1\text{Im}][\text{BF}_4]$ from the literature (i.e., heating at 10 °C/min from room temperature to 600 °C and recording the temperature of the onset of decomposition). For bulk IL, the thermal stability limit is reported in the literature to be approximately 400 °C [66], while Babucci et al. found that in the presence of powdered ZnO, it was 333 °C. The approximate thickness of the IL layer on ZnO in their work was of a similar order of magnitude as the data discussed here, at a value of 12.4 Å. They ruled out the effects of coverage on their findings since the T_{onset} value they measured

for one of the thinnest layers of IL was one of the largest values and thus attributed the decrease in thermal stability to the nature of the oxide surface, specifically its basicity. In our study, using a single-crystal ZnO (0001) surface, the decomposition of [C₄C₁Im][BF₄] occurred at a much lower temperature than the long-term thermal stability of the pure IL (~400 °C) and of IL on powdered ZnO (~300 °C), suggesting that the nature of the oxide surface is very important.

Previous studies into the morphology of ZnO surfaces have shown that the ZnO (0001)–Zn surface is covered with terraces of triangular pits and islands with step edges that are O-terminated. The exposure of O²⁻ ions at these step edges is thought to be connected to the reactivity of the ZnO surface and, therefore, connected to reactions that take place at the surface. For example, in our study, we found that [BF₄]⁻ anions dissociated and the B atoms attached to O²⁻ ions at the step edges. As the surface was heated to 200 °C, the exposed O²⁻ ions became even more important. Upon heating, H, C, N, F and B were clearly lost from the surface as volatile products, which, along with the loss of surface oxygen, strongly suggests that H₂O, CO and NO were desorption species, as well as volatile decomposition products. These reactions led to the loss of oxygen atoms from the near-surface region, leaving a Zn-rich surface (i.e., metallisation of the surface).

The interactions of ILs on oxide surfaces have significant consequences for potential applications involving ILs and oxides, such as catalysis and photovoltaics. A reduction in the thermal stability of 1-alkyl-*n*-imidazolium tetrafluoroborate ILs on ZnO may have a negative impact on the effectiveness of ZnO-based catalysts (such as SILP and SCILL) at higher temperatures. It may also be detrimental for the use of ILs in ZnO-based photovoltaic systems, where extensive solar heating could result in significant breakdown of the IL and, ultimately, the breakdown of the photovoltaic device. Since the reactivity of ILs is tuneable, if the tetrafluoroborate anion (which is relatively reactive) was replaced by a less reactive anion, then it is possible that the observed reaction with the ZnO surface may be reduced or eliminated. There is also the possibility of altering the structure of ZnO to improve stability at the ZnO/IL interface; however, this would affect optical transitions, which is not desirable. Since the tetrafluoroborate anion is fairly hydrophilic, replacing it with a more hydrophobic anion (such as bis(trifluorosulfonyl)imide) might give a more desirable result for avoiding degradation. If the ZnO surface catalyses the reaction between the [BF₄]⁻ ion and water, it could be that any IL containing B-F or C-F bonds (i.e., the bis(trifluorosulfonyl)imide anion) are at risk of reaction with water in the presence of a ZnO surface. In this case, fluorine-free ILs may be a more suitable choice to avoid degradation. It would be an interesting experimental and/or computational study to look at different combinations of cations and anions on ZnO in terms of their interfacial reactions and in terms of their energy level alignment to find the best choice of IL for ZnO-based devices.

5. Conclusions

The adsorption of [C₈C₁Im][BF₄] on polar ZnO (0001) and non-polar ZnO (10 $\bar{1}$ 0) surfaces was studied using synchrotron-based soft XPS. The IL is deposited mostly intact on the ZnO (0001) surface, but with some dissociation of [BF₄]⁻ anions, resulting in boron atoms attaching to oxygen atoms in the ZnO surface and forming B₂O₃. The deposition of [C₈C₁Im][BF₄] on the ZnO (10 $\bar{1}$ 0) surface at –150 °C resulted in the appearance of more chemical environments in the XPS spectra. We propose that the high temperature of the IL evaporator caused some conversion of [C₈C₁Im][BF₄] to a carbene–borane adduct, resulting in the deposition of both the IL and adduct onto the ZnO surface.

The thermal stability of [C₄C₁Im][BF₄] on the polar ZnO (0001) surface was investigated using synchrotron-based soft XPS at normal and grazing emission angles from –150 °C to 200 °C. It was found that [C₄C₁Im][BF₄] is deposited mostly intact at –150 °C.

Changes in the C 1s spectra as the surface was heated through the glass transition temperature of the IL indicate a phase change in the IL from a glassy solid to a liquid. The reduction in intensity of C 1s, N 1s, F 1s and B 1s spectra as the surface was heated to room temperature suggests the IL forms islands on the ZnO surface. The most significant changes in the XPS spectra occur as the surface is heated to 88 °C, indicating desorption of the IL islands and an increase in degradation and reactions at the ZnO surface. The decomposition of [C₄C₁Im][BF₄] on the ZnO (0001) surface occurs at a much lower temperature than the long-term thermal stability of the pure IL, quoted in the literature as ~400 °C, and of IL on powdered ZnO, quoted in the literature as ~300 °C. This indicates that the ZnO (0001) surface may catalyse the thermal decomposition of [C₄C₁Im][BF₄] at lower temperatures. This extreme reduction in thermal stability may have negative consequences for the use of ILs in ZnO-based photovoltaic systems, where operating temperatures can routinely reach 80 °C.

Supplementary Materials: The following supporting information can be downloaded at <https://www.mdpi.com/article/10.3390/surfaces8020029/s1>, Figure S1: XPS surveys of clean ZnO (0001) (photon energy, $h\nu = 700$ eV) (a), and of clean ZnO (10 $\bar{1}0$) ($h\nu = 800$ eV) (b); Figure S2: LEED patterns taken from the ZnO (0001) single crystal surfaces at the ANTARES beamline (left) and the AU-MatLine beamline (right); Figure S3: Side view (left) and top-down view (right) of the modified Knudsen cell. Prior to being bolted onto the vacuum chamber, a small amount (typically <1 mL) of IL is placed into a small quartz vial (not shown) which fits down the central column. The heating element consists of tantalum wire weaved through the column wall; Figure S4: O 1s spectra of [C₈C₁Im][BF₄] on ZnO (0001) (blue curve) and ZnO (10 $\bar{1}0$) (red curve) at –150 °C. Fitted components are shown by dashed lines and the resultant envelope is shown by a darker solid line. The O 1s region is normalised to the largest component at 530.0 eV. The other XPS regions in the main paper were calibrated to the ZnO lattice peak at 530.0 eV. The photon energy used for the O 1s region was 700 eV; Figure S5: C 1s spectra recorded at normal emission NE (left) and area of the C 1s region fit to each spectrum (right) for [C₄C₁Im][BF₄] on ZnO (0001) for temperatures –150 °C, –80 °C, room temperature (RT), 88 °C and 200 °C. The C 1s spectra have not been normalised, the intensity is the counts per second from the raw data; Figure S6: N 1s spectra recorded at grazing emission GE (left) and area of the N 1s region fit to each spectrum (right) for [C₄C₁Im][BF₄] on ZnO (0001) for temperatures –150 °C, –80 °C, room temperature (RT) and 88 °C. GE was chosen to show the intensity changes over more temperatures (NE data was only up to RT). The N 1s spectra have not been normalised, the intensity shown is the counts per second from the raw data; Figure S7: F 1s spectra recorded at normal emission NE (left) and area of the F 1s region fit to each spectrum (right) for [C₄C₁Im][BF₄] on ZnO (0001) for temperatures –150 °C, –80 °C, room temperature (RT), 88 °C and 200 °C. The F 1s spectra have not been normalised, the intensity shown is the counts per second from the raw data; Figure S8: B 1s spectra recorded at normal emission NE (left) and area of the B 1s region fit to each spectrum (right) for [C₄C₁Im][BF₄] on ZnO (0001) for temperatures –150 °C, –80 °C, room temperature (RT), 88 °C and 200 °C. The B 1s spectra have not been normalised, the intensity shown is the counts per second from the raw data; Figure S9: O 1s spectra recorded at normal emission NE (left) and area of the O 1s region fit to each spectrum (right) for [C₄C₁Im][BF₄] on ZnO (0001) for temperatures –150 °C, –80 °C, room temperature (RT), 88 °C and 200 °C. The O 1s spectra have not been normalised, the intensity shown is the counts per second from the raw data. Table S1: Calculated thickness of IL depositions on ZnO; Table S2: Binding energies and assignments of peaks fitted to the O 1s spectra of [C₈C₁Im][BF₄] on ZnO (0001) and (10 $\bar{1}0$); Table S3: Binding energies and assignments of peaks fitted to the C 1s spectra of [C₄C₁Im][BF₄] on ZnO (0001) at –150 °C, –80 °C and room temperature (RT) at normal emission (NE) and grazing emission (GE); Table S4: Binding energies and assignments of peaks fitted to the N 1s spectra of [C₄C₁Im][BF₄] on ZnO (0001) at –150 °C, –80 °C, room temperature (RT) and 88 °C at normal emission (NE) and grazing emission (GE); Table S5: Binding energies and assignments of peaks fitted to the F 1s spectra of [C₄C₁Im][BF₄] on ZnO (0001) at –150 °C, –80 °C, room temperature (RT), 88 °C and 200 °C at normal emission

(NE) and grazing emission (GE); Table S6: Binding energies and assignments of peaks fitted to the B 1s spectra of [C₄C₁Im][BF₄] on ZnO (0001) at −150 °C, −80 °C, room temperature (RT), 88 °C and 200 °C at normal emission (NE) and grazing emission (GE); Table S7: Binding energies and assignments of peaks fitted to the O 1s spectra of [C₄C₁Im][BF₄] on ZnO (0001) at room temperature (RT), 88 °C and 200 °C at normal emission (NE) and grazing emission (GE) [72–80].

Author Contributions: Conceptualization, R.G.J. and K.L.S.; formal analysis, Z.H., J.C. and K.L.S.; funding acquisition, R.G.J. and K.L.S.; investigation, Z.H., A.G.T., R.G.J., M.W., J.A., M.C.A., Z.L. and K.L.S.; project administration, K.L.S.; resources, J.A., M.C.A. and Z.L.; writing—original draft, Z.H.; writing—review and editing, R.G.J., M.W. and K.L.S. All authors have read and agreed to the published version of the manuscript.

Funding: The authors gratefully acknowledge beam time awarded at the ANTARES beamline at SOLEIL synchrotron in France under proposal 20120835 and beam time awarded at the AU-MATLine beamline at ASTRID2 facility at Aarhus University in Denmark under proposal ISA-16-1042. The experimental work at ANTARES was funded under The European Community's Seventh Framework Programme (FP7/2007-2013) under grant agreement no. 226716. KLS and RGJ gratefully acknowledge funding from the Engineering and Physical Science Research Council, U.K. (EP/I018093/1). The present work has also been partially supported by the project TED2021-132656B-C21 granted by the Call 2021—“Ecological Transition and Digital Transition Projects” promoted by the Ministry of Science and Innovation, funded by the European Union within the “NextGeneration” EU 23 program; the Recovery, Transformation, and Resilience Plan; and the State Investigation Agency.

Data Availability Statement: The data that support the findings of this study are openly available at the following URL/DOI: <https://uclandata.uclan.ac.uk/id/eprint/537> (accessed on 19 February 2025).

Acknowledgments: We thank Maria Torres-Molina for helping to conduct the experiments at AU-MATLine. Z.H. and J.C. acknowledge PhD studentships from the Jeremiah Horrocks Institute for Mathematics, Physics and Astronomy.

Conflicts of Interest: Authors María C. Asensio, Zoë Henderson, and Jordan Cole are employed by the GREENER Group, NSG Group and Nanoco Technologies Ltd., respectively. The authors declare that the research was conducted in the absence of any commercial or financial relationships that could be construed as a potential conflict of interest.

References

1. Özgür, Ü.; Alivov, Y.I.; Liu, C.; Teke, A.; Reshchikov, M.A.; Doğan, S.; Avrutin, V.; Cho, S.J.; Morkoç, H. A Comprehensive Review of ZnO Materials and Devices. *J. Appl. Phys.* **2005**, *98*, 041301. [CrossRef]
2. Huang, J.; Yin, Z.; Zheng, Q. Applications of ZnO in Organic and Hybrid Solar Cells. *Energy Environ. Sci.* **2011**, *4*, 3861–3877. [CrossRef]
3. Choi, Y.; Futagami, K.; Fujitani, T.; Nakamura, J. The Role of ZnO in Cu/ZnO Methanol Synthesis Catalysts—Morphology Effect or Active Site Model? *Appl. Catal. A Gen.* **2001**, *208*, 163–167. [CrossRef]
4. Lee, K.M.; Lai, C.W.; Ngai, K.S.; Juan, J.C. Recent Developments of Zinc Oxide Based Photocatalyst in Water Treatment Technology: A Review. *Water Res.* **2016**, *88*, 428–448. [CrossRef]
5. Loutzenhiser, P.G.; Meier, A.; Steinfeld, A. Review of the Two-Step H₂O/CO₂-Splitting Solar Thermochemical Cycle Based on Zn/ZnO Redox Reactions. *Materials* **2010**, *3*, 4922–4938. [CrossRef]
6. Park, J.S.; Lee, B.R.; Lee, J.M.; Kim, J.-S.; Kim, S.O.; Song, M.H. Efficient Hybrid Organic-Inorganic Light Emitting Diodes with Self-Assembled Dipole Molecule Deposited Metal Oxides. *Appl. Phys. Lett.* **2010**, *96*, 243306. [CrossRef]
7. Lee, B.R.; Choi, H.; SunPark, J.; Lee, H.J.; Kim, S.O.; Kim, J.Y.; Song, M.H. Surface Modification of Metal Oxide Using Ionic Liquid Molecules in Hybrid Organic-Inorganic Optoelectronic Devices. *J. Mater. Chem.* **2011**, *21*, 2051–2053. [CrossRef]
8. Harikisun, R.; Desilvestro, H. Long-Term Stability of Dye Solar Cells. *Sol. Energy* **2011**, *85*, 1179–1188. [CrossRef]
9. Kroon, J.M.; Bakker, N.J.; Smit, H.J.P.; Liska, P.; Thampi, K.R.; Wang, P.; Zakeeruddin, S.M.; Grätzel, M.; Hinsch, A.; Hore, S.; et al. Nanocrystalline Dye-Sensitized Solar Cells Having Maximum Performance. *Prog. Photovolt. Res. Appl.* **2007**, *15*, 1–18. [CrossRef]
10. Grätzel, M. Photovoltaic Performance and Long-Term Stability of Dye-Sensitized Mesoscopic Solar Cells. *Comptes Rendus Chim.* **2006**, *9*, 578–583. [CrossRef]

11. Sobota, M.; Schmid, M.; Happel, M.; Amende, M.; Maier, F.; Steinrück, H.-P.; Paape, N.; Wasserscheid, P.; Laurin, M.; Gottfried, J.M.; et al. Ionic Liquid Based Model Catalysis: Interaction of [Bmim][Tf₂n] with Pd Nanoparticles Supported on an Ordered Alumina Film. *Phys. Chem. Chem. Phys.* **2010**, *12*, 10610–10621. [[CrossRef](#)] [[PubMed](#)]
12. Sobota, M.; Happel, M.; Amende, M.; Paape, N.; Wasserscheid, P.; Laurin, M.; Libuda, J. Ligand Effects in Scill Model Systems: Site-Specific Interactions with Pt and Pd Nanoparticles. *Adv. Mater.* **2011**, *23*, 2617–2621. [[CrossRef](#)] [[PubMed](#)]
13. Dulub, O.; Boatner, L.A.; Diebold, U. Stm Study of the Geometric and Electronic Structure of ZnO (0001)-Zn₂O₃(1010), and (1120) Surfaces. *Surf. Sci.* **2002**, *519*, 201–217. [[CrossRef](#)]
14. Dulub, O.; Diebold, U.; Kresse, G. Novel Stabilization Mechanism on Polar Surfaces: ZnO(0001)-Zn. *Phys. Rev. Lett.* **2003**, *90*, 016102. [[CrossRef](#)]
15. Batyrev, E.D.; van den Heuvel, J.C. Modification of the ZnO(0001)-Zn Surface under Reducing Conditions. *Phys. Chem. Chem. Phys.* **2011**, *13*, 13127–13134. [[CrossRef](#)]
16. Fujimura, N.; Nishihara, T.; Goto, S.; Xu, J.; Ito, T. Control of Preferred Orientation for ZnOx Films: Control of Self-Texture. *J. Cryst. Growth* **1993**, *130*, 269–279. [[CrossRef](#)]
17. Cole, J.; Syres, K.L. Ionic Liquids on Oxide Surfaces. *J. Phys. Condens. Matter* **2022**, *34*, 213002. [[CrossRef](#)]
18. Kanai, M.; Watanabe, K.; Maruyama, S.; Matsumoto, Y. Ionic Liquid/ZnO(0001) Single Crystal and Epitaxial Film Interfaces Studied through a Combination of Electrochemical Measurements and a Pulsed Laser Deposition Process under Vacuum. *Phys. Chem. Chem. Phys.* **2019**, *21*, 25506–25512. [[CrossRef](#)]
19. Avila, J.; Razado-Colambo, I.; Lorcy, S.; Lagarde, B.; Giorgetta, J.-L.; Polack, F.; Asensio, M.C. Antares, a Scanning Photoemission Microscopy Beamline at Soleil. *J. Phys. Conf. Ser.* **2013**, *425*, 192023. [[CrossRef](#)]
20. Bianchi, M.; Hofmann, P.; Hoffmann, S.V.; Jones, N.C.; Li, Z.; Miwa, J.A.; Møller, S.P.; Nielsen, J.S.; Thomsen, H.D.; Ulstrup, S.; et al. Status and Strategy at Isa, Centre for Storage Ring Facilities, Aarhus University, Denmark. *Eur. Phys. J. Plus* **2023**, *138*, 132. [[CrossRef](#)]
21. Seah, M.P. An Accurate and Simple Universal Curve for the Energy-Dependent Electron Inelastic Mean Free Path. *Surf. Interface Anal.* **2012**, *44*, 497–503. [[CrossRef](#)]
22. Watts, J.F.; Wolstenholme, J. *An Introduction to Surface Analysis by XPS and AES*; John Wiley & Sons: Hoboken, NJ, USA, 2003.
23. McLean, B.; Li, H.; Stefanovic, R.; Wood, R.J.; Webber, G.B.; Ueno, K.; Watanabe, M.; Warr, G.G.; Page, A.; Atkin, R. Nanostructure of [Li(G4)] TFSI and [Li(G4)] No₃ Solvate Ionic Liquids at HOPG and Au(111) Electrode Interfaces as a Function of Potential. *Phys. Chem. Chem. Phys.* **2015**, *17*, 325–333. [[CrossRef](#)] [[PubMed](#)]
24. Valtiner, M.; Borodin, S.; Grundmeier, G. Preparation and Characterisation of Hydroxide Stabilised ZnO(0001)-Zn-OH Surfaces. *Phys. Chem. Chem. Phys.* **2007**, *9*, 2406–2412. [[CrossRef](#)] [[PubMed](#)]
25. Henderson, Z.; Walton, A.S.; Thomas, A.G.; Syres, K.L. Water-Induced Reordering in Ultrathin Ionic Liquid Films. *J. Phys. Condens. Matter* **2018**, *30*, 334003. [[CrossRef](#)]
26. Huddleston, J.G.; Visser, A.E.; Reichert, W.M.; Willauer, H.D.; Broker, G.A.; Rogers, R.D. Characterization and Comparison of Hydrophilic and Hydrophobic Room Temperature Ionic Liquids Incorporating the Imidazolium Cation. *Green Chem.* **2001**, *3*, 156–164. [[CrossRef](#)]
27. Jablonski, A.; Powell, C.J. Information Depth and the Mean Escape Depth in Auger Electron Spectroscopy and X-Ray Photoelectron Spectroscopy. *J. Vac. Sci. Technol. A* **2002**, *21*, 274–283. [[CrossRef](#)]
28. Parhi, P.; Manivannan, V. Novel Microwave Initiated Synthesis of Zn₂SiO₄ and MCrO₄ (M= Ca, Sr, Ba, Pb). *J. Alloys Compd.* **2009**, *469*, 558–564. [[CrossRef](#)]
29. Villar-Garcia, I.J.; Smith, E.F.; Taylor, A.W.; Qiu, F.; Lovelock, K.R.J.; Jones, R.G.; Licence, P. Charging of Ionic Liquid Surfaces under X-Ray Irradiation: The Measurement of Absolute Binding Energies by XPS. *Phys. Chem. Chem. Phys.* **2011**, *13*, 2797–2808. [[CrossRef](#)]
30. Gannon, T.J.; Law, G.; Watson, P.R.; Carmichael, A.J.; Seddon, K.R. First Observation of Molecular Composition and Orientation at the Surface of a Room-Temperature Ionic Liquid. *Langmuir* **1999**, *15*, 8429–8434. [[CrossRef](#)]
31. Jeon, Y.; Sung, J.; Bu, W.; Vaknin, D.; Ouchi, Y.; Kim, D. Interfacial Restructuring of Ionic Liquids Determined by Sum-Frequency Generation Spectroscopy and X-Ray Reflectivity. *J. Phys. Chem. C* **2008**, *112*, 19649–19654. [[CrossRef](#)]
32. Lockett, V.; Sedev, R.; Bassell, C.; Ralston, J. Angle-Resolved X-Ray Photoelectron Spectroscopy of the Surface of Imidazolium Ionic Liquids. *Phys. Chem. Chem. Phys.* **2008**, *10*, 1330–1335. [[CrossRef](#)] [[PubMed](#)]
33. Lynden-Bell, R.M.; Del Popolo, M. Simulation of the Surface Structure of Butylmethylimidazolium Ionic Liquids. *Phys. Chem. Chem. Phys.* **2006**, *8*, 949–954. [[CrossRef](#)] [[PubMed](#)]
34. Taylor, A.W.; Lovelock, K.R.J.; Jones, R.G.; Licence, P. Borane-Substituted Imidazol-2-Ylidenes: Syntheses in Vacuo. *Dalton Trans.* **2011**, *40*, 1463–1470. [[CrossRef](#)] [[PubMed](#)]
35. Wagstaffe, M.; Jackman, M.J.; Syres, K.L.; Generalov, A.; Thomas, A.G. Ionic Liquid Ordering at an Oxide Surface. *ChemPhysChem* **2016**, *17*, 3430–3434. [[CrossRef](#)]

36. Southam, A. (University of Nottingham, Nottingham, UK). Surface Synthesis; the Ullman Reaction with an Ionic Liquid, 2017. (Unpublished work).
37. Lv, Y.; Huang, S.; Lu, S.; Ding, W.; Yu, X.; Liang, G.; Zou, J.; Kang, F.; Zhang, J.; Cao, Y. B₂O₃/LiBO₂ Dual-Modification Layer Stabilized Ni-Rich Cathode for Lithium-Ion Battery. *J. Power Sources* **2022**, *536*, 231510. [[CrossRef](#)]
38. Smith, E.F.; Rutten, F.J.; Villar-Garcia, I.J.; Briggs, D.; Licence, P. Ionic Liquids in Vacuo: Analysis of Liquid Surfaces Using Ultra-High-Vacuum Techniques. *Langmuir* **2006**, *22*, 9386–9392. [[CrossRef](#)]
39. Dorn, R.; Lüth, H. The Adsorption of Oxygen and Carbon Monoxide on Cleaved Polar and Nonpolar ZnO Surfaces Studied by Electron Energy Loss Spectroscopy. *Surf. Sci.* **1977**, *68*, 385–391. [[CrossRef](#)]
40. Raupp, G.; Dumesic, J. Adsorption of Carbon Monoxide, Carbon Dioxide, Hydrogen, and Water on Titania Surfaces with Different Oxidation States. *J. Phys. Chem.* **1985**, *89*, 5240–5246. [[CrossRef](#)]
41. Klaver, T.P.C.; Luppi, M.; Sluiter, M.H.F.; Kroon, M.C.; Thijsse, B.J. DFT Study of 1,3-Dimethylimidazolium Tetrafluoroborate on Al and Cu(111) Surfaces. *J. Phys. Chem. C* **2011**, *115*, 14718–14730. [[CrossRef](#)]
42. Meusel, M.; Lexow, M.; Gezmis, A.; Bayer, A.; Maier, F.; Steinrück, H.-P. Growth of Multilayers of Ionic Liquids on Au(111) Investigated by Atomic Force Microscopy in Ultrahigh Vacuum. *Langmuir* **2020**, *36*, 13670–13681. [[CrossRef](#)]
43. Syres, K.L.; Jones, R.G. Adsorption, Desorption, and Reaction of 1-Octyl-3-Methylimidazolium Tetrafluoroborate, [C₈C₁Im][BF₄], Ionic Liquid Multilayers on Cu (111). *Langmuir* **2015**, *31*, 9799–9808. [[CrossRef](#)] [[PubMed](#)]
44. Uhl, B.; Buchner, F.; Gabler, S.; Bozorgchenani, M.; Jürgen Behm, R. Adsorption and Reaction of Sub-Monolayer Films of an Ionic Liquid on Cu(111). *Chem. Commun.* **2014**, *50*, 8601–8604. [[CrossRef](#)] [[PubMed](#)]
45. Babucci, M.; Balci, V.; Akçay, A.; Uzun, A. Interactions of [BMIM][BF₄] with Metal Oxides and Their Consequences on Stability Limits. *J. Phys. Chem. C* **2016**, *120*, 20089–20102. [[CrossRef](#)]
46. Ohtani, H.; Ishimura, S.; Kumai, M. Thermal Decomposition Behaviors of Imidazolium-Type Ionic Liquids Studied by Pyrolysis-Gas Chromatography. *Anal. Sci.* **2008**, *24*, 1335–1340. [[CrossRef](#)]
47. Kroon, M.C.; Buijjs, W.; Peters, C.J.; Witkamp, G.J. Quantum Chemical Aided Prediction of the Thermal Decomposition Mechanisms and Temperatures of Ionic Liquids. *Thermochim. Acta* **2007**, *465*, 40–47. [[CrossRef](#)]
48. Coppa, B.; Davis, R.; Nemanich, R. Gold Schottky Contacts on Oxygen Plasma-Treated, N-Type ZnO (0001). *Appl. Phys. Lett.* **2003**, *82*, 400–402. [[CrossRef](#)]
49. Asakuma, N.; Fukui, T.; Toki, M.; Awazu, K.; Imai, H. Photoinduced Hydroxylation at ZnO Surface. *Thin Solid Film.* **2003**, *445*, 284–287. [[CrossRef](#)]
50. Heinhold, R.; Williams, G.; Cooil, S.; Evans, D.; Allen, M. Influence of Polarity and Hydroxyl Termination on the Band Bending at ZnO Surfaces. *Phys. Rev. B* **2013**, *88*, 235315. [[CrossRef](#)]
51. Deyko, A.; Jones, R.G. Adsorption, Absorption and Desorption of Gases at Liquid Surfaces: Water [C₈C₁Im][BF₄] and [C₂C₁Im][Tf₂N]. *Faraday Discuss.* **2012**, *154*, 265–288. [[CrossRef](#)]
52. Allen, M.; Zemlyanov, D.; Waterhouse, G.; Metson, J.; Veal, T.D.; McConville, C.F.; Durbin, S. Polarity Effects in the X-Ray Photoemission of ZnO and Other Wurtzite Semiconductors. *Appl. Phys. Lett.* **2011**, *98*, 101906. [[CrossRef](#)]
53. Becker, T.H.; Kunat, M.; Boas, C.; Burghaus, U.; Wöll, C. Adsorption Dynamics of Co on the Polar Surfaces of ZnO. *J. Chem. Phys.* **2000**, *113*, 6334–6343. [[CrossRef](#)]
54. Au, C.T.; Hirsch, W.; Hirschwald, W. Adsorption and Interaction of Carbon Dioxide, Formic Acid and Hydrogen/Carbon Dioxide Mixtures on (1010) Zinc Oxide Surfaces Studied by Photoelectron Spectroscopy (XPS and UPS). *Surf. Sci.* **1988**, *199*, 507–517. [[CrossRef](#)]
55. Vai, A.T.; Kuznetsov, V.L.; Dilworth, J.R.; Edwards, P.P. Uv-Induced Improvement in ZnO Thin Film Conductivity: A New in Situ Approach. *J. Mater. Chem. C* **2014**, *2*, 9643–9652. [[CrossRef](#)]
56. Lovelock, K.R.J.; Smith, E.F.; Deyko, A.; Villar-Garcia, I.J.; Licence, P.; Jones, R.G. Water Adsorption on a Liquid Surface. *Chem. Commun.* **2007**, *46*, 4866–4868. [[CrossRef](#)]
57. Brow, R.K. An XPS Study of Oxygen Bonding in Zinc Phosphate and Zinc Borophosphate Glasses. *J. Non-Cryst. Solids* **1996**, *194*, 267–273. [[CrossRef](#)]
58. Rivera-Rubero, S.; Baldelli, S. Influence of Water on the Surface of Hydrophilic and Hydrophobic Room-Temperature Ionic Liquids. *J. Am. Chem. Soc.* **2004**, *126*, 11788–11789. [[CrossRef](#)]
59. Rivera-Rubero, S.; Baldelli, S. Influence of Water on the Surface of the Water-Miscible Ionic Liquid 1-Butyl-3-Methylimidazolium Tetrafluoroborate: A Sum Frequency Generation Analysis. *J. Phys. Chem. B* **2006**, *110*, 15499–15505. [[CrossRef](#)]
60. Holbrey, J.D.; Seddon, K.R. The Phase Behaviour of 1-Alkyl-3-Methylimidazolium Tetrafluoroborates; Ionic Liquids and Ionic Liquid Crystals. *J. Chem. Soc. Dalton Trans.* **1999**, *13*, 2133–2140. [[CrossRef](#)]
61. Fox, D.M.; Gilman, J.W.; De Long, H.C.; Trulove, P.C. Tga Decomposition Kinetics of 1-Butyl-2,3-Dimethylimidazolium Tetrafluoroborate and the Thermal Effects of Contaminants. *J. Chem. Thermodyn.* **2005**, *37*, 900–905. [[CrossRef](#)]
62. Ngo, H.L.; LeCompte, K.; Hargens, L.; McEwen, A.B. Thermal Properties of Imidazolium Ionic Liquids. *Thermochim. Acta* **2000**, *357–358*, 97–102. [[CrossRef](#)]

63. Maton, C.; De Vos, N.; Stevens, C.V. Ionic Liquid Thermal Stabilities: Decomposition Mechanisms and Analysis Tools. *Chem. Soc. Rev.* **2013**, *42*, 5963–5977. [[CrossRef](#)] [[PubMed](#)]
64. Van Valkenburg, M.E.; Vaughn, R.L.; Williams, M.; Wilkes, J.S. Thermochemistry of Ionic Liquid Heat-Transfer Fluids. *Thermochim. Acta* **2005**, *425*, 181–188. [[CrossRef](#)]
65. Kosmulski, M.; Gustafsson, J.; Rosenholm, J.B. Thermal Stability of Low Temperature Ionic Liquids Revisited. *Thermochim. Acta* **2004**, *412*, 47–53. [[CrossRef](#)]
66. Cao, Y.; Mu, T. Comprehensive Investigation on the Thermal Stability of 66 Ionic Liquids by Thermogravimetric Analysis. *Ind. Eng. Chem. Res.* **2014**, *53*, 8651–8664. [[CrossRef](#)]
67. Deyko, A.; Lovelock, K.R.J.; Licence, P.; Jones, R.G. The Vapour of Imidazolium-Based Ionic Liquids: A Mass Spectrometry Study. *Phys. Chem. Chem. Phys.* **2011**, *13*, 16841–16850. [[CrossRef](#)]
68. Lovelock, K.R.J.; Deyko, A.; Licence, P.; Jones, R.G. Vaporisation of an Ionic Liquid near Room Temperature. *Phys. Chem. Chem. Phys.* **2010**, *12*, 8893–8901. [[CrossRef](#)]
69. Vohs, J.; Barteau, M. Conversion of Methanol, Formaldehyde and Formic Acid on the Polar Faces of Zinc Oxide. *Surf. Sci.* **1986**, *176*, 91–114. [[CrossRef](#)]
70. Zwicker, G.; Jacobil, K.; Cunningham, J. Temperature Programmed Desorption of Polar Adsorbates from (1010),(0001) and (0001) ZnO Surfaces. *Int. J. Mass Spectrom. Ion Process.* **1984**, *60*, 213–223. [[CrossRef](#)]
71. Strunk, J.; Kähler, K.; Xia, X.; Muhler, M. The Surface Chemistry of ZnO Nanoparticles Applied as Heterogeneous Catalysts in Methanol Synthesis. *Surf. Sci.* **2009**, *603*, 1776–1783. [[CrossRef](#)]
72. Armstrong, J.P.; Hurst, C.; Jones, R.G.; Licence, P.; Lovelock, K.R.; Satterley, C.J.; Villar-Garcia, I.J. Vapourisation of Ionic Liquids. *Phys. Chem. Chem. Phys.* **2007**, *9*, 982–990. [[CrossRef](#)]
73. Meyer, B.; Marx, D.; Dulub, O.; Diebold, U.; Kunat, M.; Langenberg, D.; Wöll, C. Partial Dissociation of Water Leads to Stable Superstructures on the Surface of Zinc Oxide. *Angew. Chem. Int. Ed.* **2004**, *43*, 6641–6645. [[CrossRef](#)] [[PubMed](#)]
74. Broderick, A.; Khalifa, Y.; Shiflett, M.B.; Newberg, J.T. Water at the Ionic Liquid–Gas Interface Examined by Ambient Pressure X-Ray Photoelectron Spectroscopy. *J. Phys. Chem. C* **2017**, *121*, 7337–7343. [[CrossRef](#)]
75. Wöll, C. The Chemistry and Physics of Zinc Oxide Surfaces. *Prog. Surf. Sci.* **2007**, *82*, 55–120. [[CrossRef](#)]
76. Liu, Y.; Xu, W.; Shan, Y.; Xu, H. High Reactivity of the ZnO(0001) Polar Surface: The Role of Oxygen Adatoms. *J. Phys. Chem. C* **2017**, *121*, 15711–15718. [[CrossRef](#)]
77. Ma, C.; Jin, W.; Ma, X.; Han, H.; Yu, J.; Wu, Y. Water Adsorption Behaviors of High Index Polar Surfaces in ZnO. *Appl. Surf. Sci.* **2019**, *498*, 143898. [[CrossRef](#)]
78. Önsten, A.; Stoltz, D.; Palmgren, P.; Yu, S.; Göthelid, M.; Karlsson, U.O. Water Adsorption on ZnO(0001): Transition from Triangular Surface Structures to a Disordered Hydroxyl Terminated Phase. *J. Phys. Chem. C* **2010**, *114*, 11157–11161. [[CrossRef](#)]
79. Wang, Y.; Meyer, B.; Yin, X.; Kunat, M.; Langenberg, D.; Traeger, F.; Birkner, A.; Wöll, C. Hydrogen Induced Metallicity on the ZnO(10-10) Surface. *Phys. Rev. Lett.* **2005**, *95*, 266104. [[CrossRef](#)]
80. Wang, Y.; Muhler, M.; Wöll, C. Spectroscopic Evidence for the Partial Dissociation of H₂O on ZnO(10 $\bar{1}$ 0). *Phys. Chem. Chem. Phys.* **2006**, *8*, 1521–1524. [[CrossRef](#)]

Disclaimer/Publisher’s Note: The statements, opinions and data contained in all publications are solely those of the individual author(s) and contributor(s) and not of MDPI and/or the editor(s). MDPI and/or the editor(s) disclaim responsibility for any injury to people or property resulting from any ideas, methods, instructions or products referred to in the content.